Close-range blast loading on empty recyclable metal beverage cans for use in sacrificial cladding structure

Sivakumar Palanivelu[1*], Wim Van Paepegem[1], Joris Degrieck[1], Bruno Reymen[2], Jean-Marie Ndambi[2], John Vantomme[2], Dimitrios Kakogiannis[3], Jan Wastiels[3], Danny Van Hemelrijck[3]

[1]Department of Materials Science and Engineering, Ghent University, Sint-Pietersnieuwstraat 41, 9000 Gent, Belgium
[2]Royal Military Academy, Civil and Materials Engineering Department, Building G, Level 0, 8 Av. Hobbema B-1000, Brussels, Belgium
[3]Department of Mechanics of Materials and Constructions, Vrije Universiteit Brussel, Pleinlaan 2 B-1050 Brussels, Belgium

Abstract

This article deals with the experimental and numerical blast study on a single empty recyclable metal beverage cans. The idea is to make a macro-foam (sacrificial cladding structure) out of these cans to protect the main load bearing members of civil engineering structures from the air blast load. Close-range free air blast tests have been conducted to understand the crushing behaviour and the energy absorption of a single empty beverage can in detail. To conduct such an air blast test a special small-scale test set-up was designed and manufactured. The effect of skin plate surface area and its nature on the blast parameters is studied. Furthermore, the effect of inertia of the skin plate on the crushing performance of the beverage can is evaluated. Tests have been conducted with different plates (made of aluminium and sandwich composite materials) with different masses which represented the skin plate of the proposed sacrificial structure. The measured blast parameters from the experimental tests were compared with ConWep predicted data. Furthermore, the influence of the finite surface area of the skin plate on the clearing of the reflected pressure waves was also studied. The deformation behaviour and the corresponding energy absorption of empty beverage cans were captured. During the experimental blast tests it was observed that a part of the total reflected impulse was lost before it transfers to the non-sacrificial structure. Hence, in order to investigate this phenomenon an Eulerian-Lagrangian coupled analyses were conducted using Hydrocodes. The results from these analyses showed that the diffraction and ground reflected pressure wave caused the loss in impulse. The results from the numerical studies have been compared and validated with the experimental results.

KEYWORDS: Blast loading; Sacrificial structure; Empty beverage can; Reflected pressure wave; Clearing effect; Impulse; Energy; Hydrocodes; Equation of state; Coupled Eulerian and Lagrangian algorithm

1. Introduction

The entire world faces the problem of security for industrial, military and civil engineering structures due to terrorist activities. The failure of the critical load bearing members such as beams, pillars, columns etc., and its debris cause major human casualties. Hence, a preventive solution is needed to safeguard the civil engineering structures and to avoid human casualties due to explosion. Out of many proposed solutions, the concept of sacrificial cladding design [1-4] has attracted more attention in terms of its functionality and its predictable behaviour. Any sacrificial cladding structure can have two layers (an inner core and an outer skin plate). The function of the skin plate is to distribute the blast pressure more evenly to the inner core which deforms progressively and absorbs most of the energy from the blast load, so that the main load bearing members of the civil engineering structures will be safeguarded. In order to safeguard the main load bearing members of the civil engineering structures, the failure load of the sacrificial cladding structure should be kept as low as possible. Keeping a lower failure load for the inner core may attribute to achieve the plastic deformation during an explosion event and so the transferred peak force to the non-sacrificial structure can be minimised.

*Corresponding author: Sivakumar Palanivelu, Tel: +32-(0)9-264.33.15, Fax: +32-(0)9-264.35.87
Email: Sivakumar.Palanivelu@UGent.be

Few researchers have proposed versatile solutions to the above problem. Guruprasad and Mukherjee [1, 2] have suggested a solution with layered mild steel plates. The results of their air blast experiments showed the perfect plastic collapse behaviour of mild steel plates. Furthermore, they have given guidelines for the parameters which control the performance of a sacrificial structure (mode of deformation, impulse transfer to the non-sacrificial structure, energy absorption in plastic deformation and collapse space efficiency). Hanssen et al. [4] demonstrated that the ideal control of the impulse or pressure transferred to the main load bearing structure (non-sacrificial structure) by using perfectly plastic material as the sacrificial part. They have used aluminium foam with different densities as a sacrificial member. The general conclusion of this study was that the energy and impulse transfer to the non-sacrificial member increased by the surface effects of the plane panel.

Generic energy absorption devices which belong to two different categories (type I and II) based on their load-displacement curves were well studied in [5-11]. The load-displacement curve of type I is relatively “flat topped” and for type II the curve falls sharply after the peak crush load. The effect of “strain-rate factor” and the “inertia factor” on the above structures are also explained in those works. The general conclusions of the referred studies are as follows: (i) the deformation of type II structures is significantly more sensitive to the impact velocity than type I; (ii) when the total kinetic energy remains the same for all test specimens, smaller final deformations result from higher impact velocities and this phenomenon is much more significant for type II structures than type I; (iii) strain rate sensitivity and the inertia effect must be considered throughout the crushing process during an impact event. Tom and Calladine [12] studied the effect of strain rate and inertia on simple plate structures under impact loading. They explained two phases of deformation of type II structures which involves plastic compression and rotation at the plastic hinges. Karagiozova et al. [13] studied the influence of inertia effects on circular and square shells subjected to explosive loads. They showed that the initial compression phase is important for the energy absorption of these structures when the blast load was transmitted by a small attached mass. Furthermore, the inertia interaction between the attached mass and the structure was greatly influenced by the dynamic mean load of crushing. Similarly, the influence of impact velocity and the material characteristics on the dynamic buckling response of circular tubes during an axial loading (quasi-static and impact) case were studied in [14, 15]. In this work, the buckling mode to global bending was explained in terms of the material yield stress, strain hardening and the strain-rate sensitivity. This paper also proved that the energy absorption performance of circular ductile tubes with high yield stress and low strain hardening is better than the one with low yield stress and high strain hardening. Similarly, the transition from initial global bending to progressive buckling on square and circular geometries was studied in [16].

In this work, we propose empty recyclable metal beverage cans for the inner core members of the sacrificial cladding structure. The concept of the proposed sacrificial cladding structure using empty recyclable beverage cans is shown in Figure 1. This configuration can be used to protect typical civil engineering structures from air blast loading. The advantages of this sacrificial structure using empty beverage cans are: (i) environment friendly due to recyclable material (ii) it is a waste product and readily available in the market and (iii) non-corrosive due to inner lacquer and outer aesthetic coatings (iv) these cans can be adopted in different configurations of macro foam depending upon the blast loading magnitudes. As an example, two different configurations (axial and radial) of the macro foam assembly of empty beverage cans are shown in Figure 2. Before designing any sacrificial

structure in full-scale, the knowledge of the performance characteristics (peak crush load, energy absorption, deformation pattern, strain rate effect on material, etc.) of the individual sacrificial member is very important. Furthermore, the effect of skin plate variables such as the surface area, inertia and the surface roughness on the performance of the inner core has to be understood. Hence, in order to understand the performance characteristics of an individual test specimen (empty beverage can) for an air blast loading a small-scale test set-up was developed. Close-range free air blast tests have been conducted with 20g of C4 with a stand-off distance of 30 cm. The crushing characteristics and the corresponding energy absorption of the individual beverage can were studied in detail.

Normally during the analysis of a blast event, the blast reflected surfaces are considered to be infinite which will not allow any diffraction of pressure waves. Furthermore, for the simplification of analysis the exponentially decaying blast pressure can be modelled as an equivalent triangular impulse load [1, 2, 4, 17]. Calculating the specific impulse without considering the clearing of the reflected pressure waves (associated with the finite surface area of the reflected surface) will over predict the efficiency of the inner core structure. Hence, in this paper the effect of clearing of the reflected pressure waves on the specific impulse is addressed by using different surface areas of the skin plates having the same mass. When a sacrificial cladding structure is exposed to a blast pressure, an impulse loading will be transferred from the skin plate to the inner core. The transferred impulse is depending upon the surface area, inertia and bending stiffness of the skin plate. Often during the design of a sacrificial cladding structure, the above mentioned parameters are not considered. Furthermore, the effect of the nature of the reflected surface on the reflected pressure parameters is an open research area where considerable amount of study is needed. Understanding the effect of these parameters is very important for designing the sacrificial cladding structure. Hence, to study the above parameters close-range blast tests (20g of C4 with a stand-off distance of 30 cm) have been conducted with different skin plates (made of aluminium and sandwich composite materials). To simplify the study only the axial pressure loading on the test specimen is considered. From the experimental results we have observed that a part of the total reflected impulse (~30%) was lost for each case. In order to understand this phenomenon coupled analyses have been conducted using Hydrocodes. The results of these analyses are compared and validated with the experimental results.

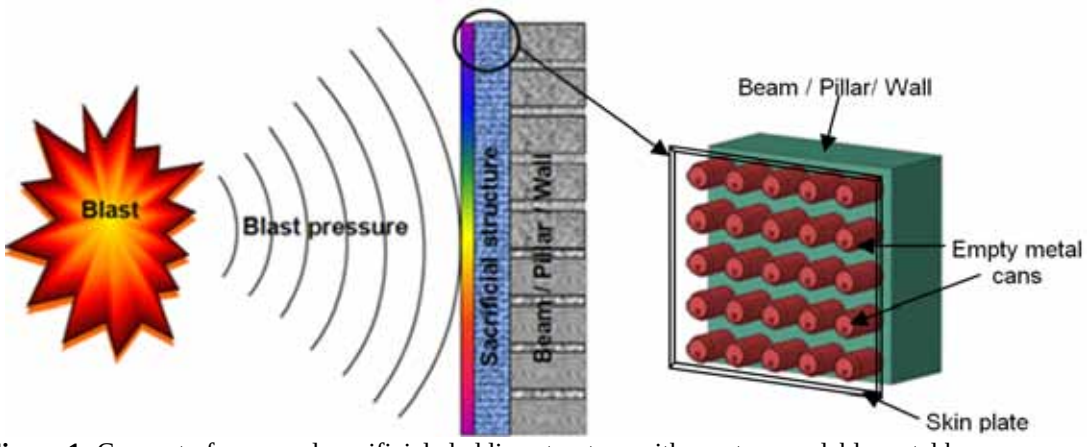

Figure 1: Concept of proposed sacrificial cladding structure with empty recyclable metal beverage cans.

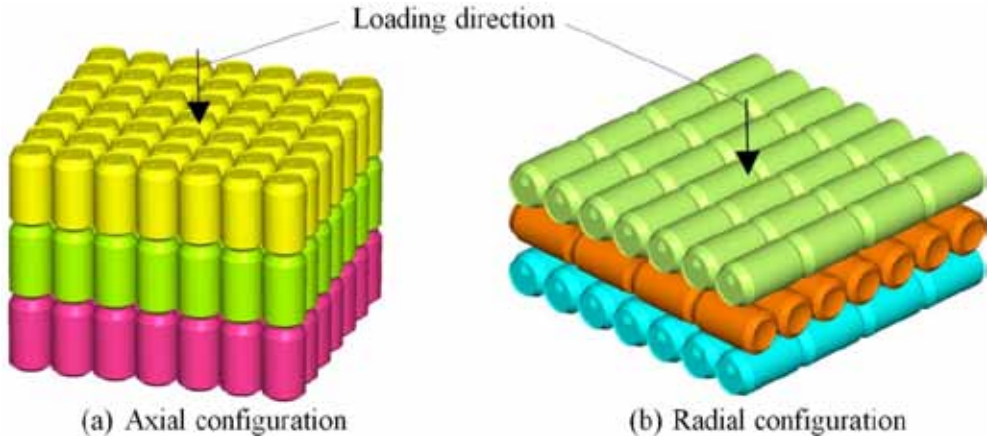

Figure 2: Two configurations of macro foam arrangement of empty recyclable metal beverage cans.

2. Test specimen and experimental set-up

2.1. Empty recyclable metal beverage cans

Used empty recyclable metal beverage cans were selected for this experimental study. Special care was taken to choose the cans without defects such as indents and scratches. The metal beverage cans available in the European market can be classified into two types based on the type of material they are made of. Type A is made of a combination of two materials; the entire body is made of steel and the top cover is made of aluminium (Figure 3(a)). Type B is completely made of aluminium. Due to the larger availability especially in Belgium, Type A was chosen for our experimental study. The measured average mass of a beverage can for this study was 26 g. The details of the geometry of an empty metal beverage can are also shown in Figure 3(b).

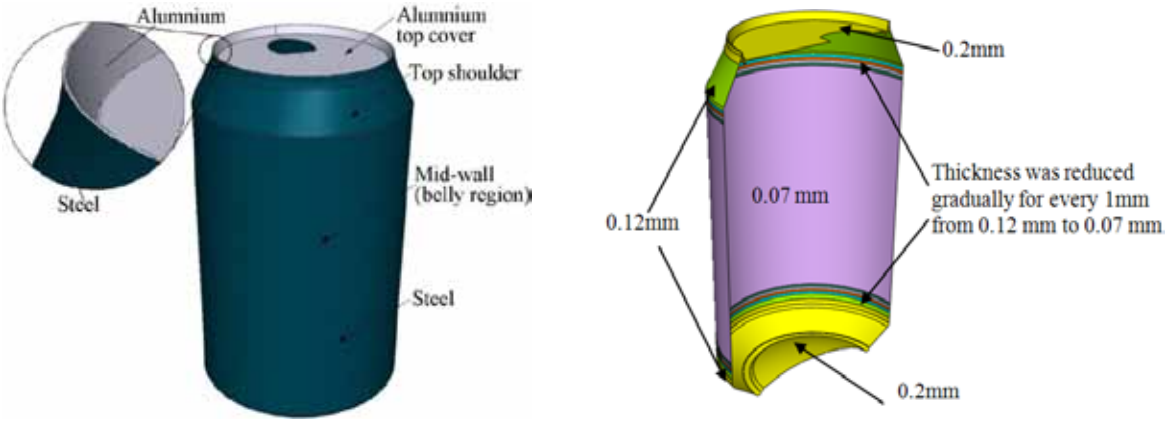

(a) Nomenclature and material details (b) Geometry details

Figure 3: Material and geometry details of an empty metal beverage can.

2.2. Experimental set-up

The schematic representation of the small-scale air blast test set-up which was used for conducting the blast tests is shown in Figure 4(a). An empty beverage can was mounted on a resting plate below which a dynamic load cell was connected to measure the transferred impulse (force-time history) to a solid copper tube. The solid copper tube which represented the non-sacrificial member was rigidly fixed to a heavy metal panel. The top cover which represents the skin plate of the sacrificial cladding structure was mounted over an empty

beverage can. The top surface was completely instrumented with an accelerometer and a pressure sensor to measure the acceleration of the skin plate and the reflected pressure from the top face of the skin plate respectively. The positions of the accelerometer and the pressure sensor were chosen close to the centre of the skin plate (70 mm from the centre of the skin plate). To simulate the real condition of air blast loading and to avoid the effect of side pressure (diffracted pressure) on the test specimen, a side cover tube was attached to the skin plate. When a test specimen deforms the side cover tube can slide over the solid copper shaft. The outer diameter of the copper tube and the inner diameter of the side tube were chosen to have an adequate clearance to avoid excessive friction between them. Semi-circular cross sectional vents were made at three locations on the copper tube throughout its length to eliminate the resistance offered by the air inside the set-up during blast loading. During the preliminary tests it was observed that the skin plates bounced from the solid copper shaft immediately after crushing of the specimen. So a steel-wired cage was made to protect the data measuring sensors. The top of the cage was covered with a nylon net which is shown in Figure 4(b).

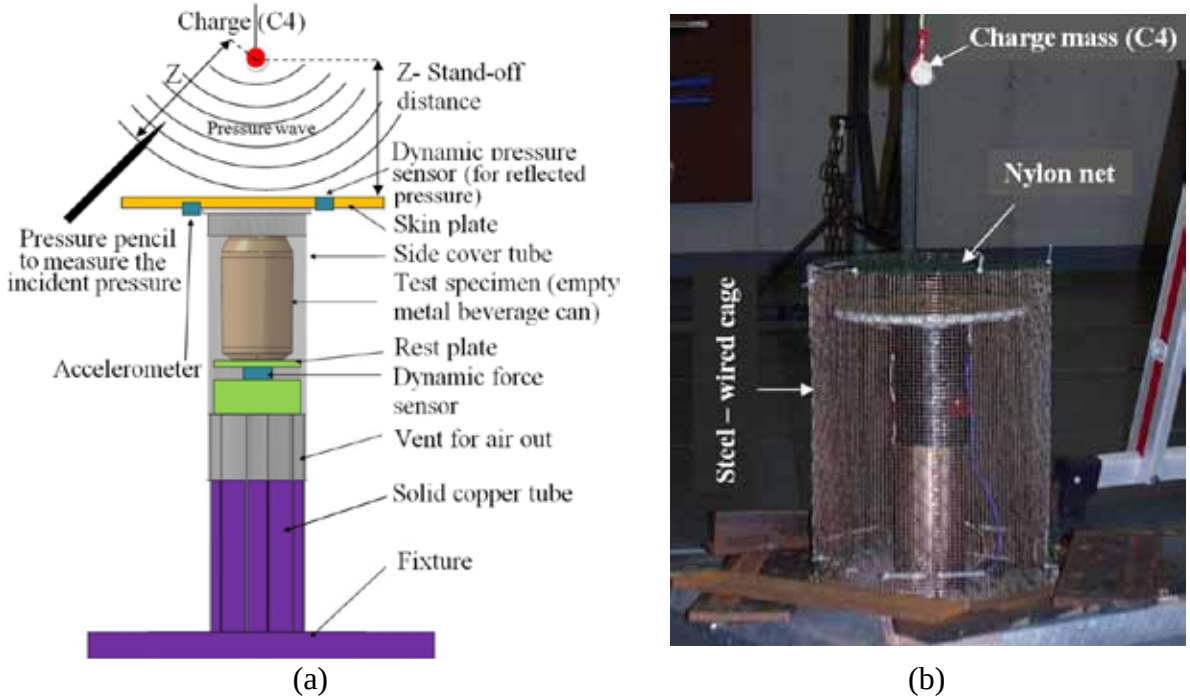

(a) (b)

Figure 4(a): Schematic view of small-scale air blast test set-up. **4(b):** Small-scale air blast set-up with steel - wired cage.

The diameter and thickness of the skin plates were chosen to restrict a maximum deflection not beyond 10 and 20 mm at the free end for aluminium and sandwich composite skin plates respectively. Totally, four skin plates have been manufactured to study the effect of surface area, nature of reflected surface and the inertia of the skin plate on the deformation length and the corresponding energy absorption of an empty beverage can. To study the effect of surface area on the blast parameters and the clearing of reflected pressure waves, two skin plates have been used with different surface area (f 200 mm and f 250 mm) having the same mass (1.0 kg). These skin plates were made with aluminium grade 2024 T3 (refer Figure 5(a) and 5(b)). In order to study the effect of the nature of the reflected surface and the inertia, in addition to the aluminium skin plate with f 250 mm, two other skin plates (f 250 mm) have been used. These skin plates were made with sandwich composite materials. The materials used for manufacturing the composite skin plates were bi-axially balanced glass

fibre mat, epoxy resin and polyurethane foam. The thickness of the top and bottom composite skin plates was in the range of 1.5 to 2.5 mm based on the mass requirement. Between the top and bottom composite plates a polyurethane foam with 7 mm thickness was used (Figure 5(c) and 5(d)). The used materials for the side covers were flexi-glass and carbon-epoxy composite for the aluminium and composite sandwich skin plates respectively. The length of the side tube was chosen 180 mm to have an adequate protection for the test specimen from the side pressure and to avoid oblique or offset loading during a blast event. To have a rigid crushing surface for the sandwich composite skin plates, a circular aluminium plate (f 97 mm; 2 mm thick) was fixed to the bottom face of the skin plate in contact with the metal beverage can. The combined inertia of the sandwich composite skin plate and the side cover tube which represented the skin plate of the sacrificial structure was 0.53 kg and 0.36 kg (Figure 5).

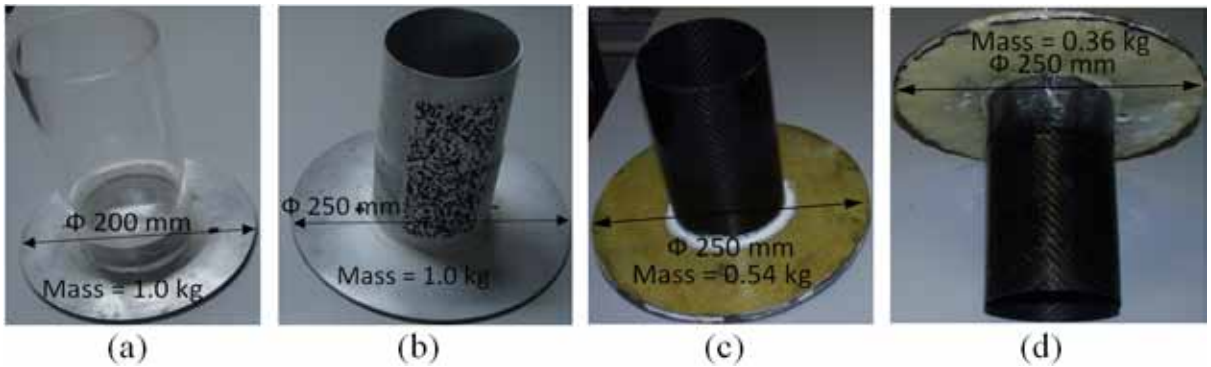

Figure 5: Aluminium and sandwich composite skin plates.

3. Experimental results and discussions

In order to understand the crushing behaviour of a single empty beverage can, a series of close-range free-air blast tests have been conducted with 20g of C4 and a stand-off distance of 30cm. The charge was made spherical in shape. To achieve a zero incidence angle of the pressure waves, the charge was placed perpendicular and positioned to the centre of the top face of the skin plate. Due to the short duration of the pressure pulse loading, a sampling frequency of 5 MHz was chosen for all sensors (pressure sensors, accelerometer and the dynamic load cell). In order to have consistent results, a minimum of five tests have been conducted for each case. The measured values of blast and material response parameters are discussed systematically in the subsequent sections.

3.1. Pressure profiles and clearing effect

3.1.1. Pressure profiles

The process of spherically charged free-air explosion can be modelled using the following Friedlander equation (1),

$$p(t) = p_{\max}\left(1 - \frac{t}{t_p}\right)\exp\left(-\frac{at}{t_p}\right) \quad (1)$$

where "t_p" is the positive phase duration and parameter "a" is the wave number (decay rate) which corresponds to the maximum pressure "P_{max}". When the blast pressure encounters an

obstruction it reflects and the reflected pressure magnitude (total) is much higher than the incident pressure magnitude. The nature of the reflected pressure is very similar to the incident pressure and it can be modelled using equation (1) with different decay rate. Often the negative phase is not considered for design of sacrificial cladding structures. Varying the input parameters of blast (mass of charge, stand-off distance and orientation to the target) and correspondingly conducting the tests for the measurement of output parameters is an expensive process which needs ample of resources. Alternatively, some commercial tools (ConWep, ATBlast, BlastX, etc.,) are available to predict the incident and reflected blast parameters for a given set of input values. However, the fully reflected blast parameters given by these programs do not include the effects of clearing of the reflected pressure wave associated with a limited size of the reflected surface. To study this effect a comparison was made between the ConWep and measured blast experimental data with different skin plates (refer Table 1). It can be seen from Table 1 that the measured blast parameters (peak reflected pressure and the corresponding positive duration) from all the skin plates do not correlate with ConWep data. The measured values of incident pressure magnitudes also gave an indication that the value predicted by ConWep is not accurate for close-range blast loading conditions (Table 1). Before conducting the blast tests with sandwich composite skin plates an analysis was carried out for the incident pressure measurement values with both aluminium skin plates (f 200 mm and f 250 mm). The standard deviation and the corresponding coefficient of variation were calculated for these 10 experiments. The calculated mean, standard deviation and the corresponding coefficient of variation (in percentage) for these experiments are 577 kPa, 10 kPa and 1.7 % respectively. These values indicated the consistency of the results and it can be acceptable for such a close-range free air blast loading conditions. Furthermore, for the design of sacrificial cladding structure the incident pressure value is not considered. Hence, the authors decided to measure the incident pressure for few experiments for the remaining skin plates such as the sandwich composite skin plates.

Table 1: Summary of blast parameters (incident and reflected).

Test No	Area of circular skin plate (A_p)	Mass of the skin plate (m_p)	Average surface roughness (R_a)	Mass of C4 (m_c)	Stand-off distance (Z)	Maximum incident over pressure (p^I_{max})	Maximum reflected over pressure (p^R_{max})	Coefficient of variation (C_v) for (p^R_{max})	Positive duration (t_p)	Coefficient of variation (C_v) for (t_p)
	m^2	Kg	µm	g	cm	kPa	kPa	%	ms	%
(Incident angle is zero)				20	30	898.7	4755	-	0.5321	-
Test 1						579	3016		0.115	
Test 2	0.0314					585	2819		0.127	
Test 3	(f	1.0	0.18	20	30	568	3002	8.6	0.119	10.7
Test 4	200mm)					580	2863		0.140	
Test 5						588	3558		0.101	
Test 1						590	4120		0.150	
Test 2	0.0491					590	3880		0.147	
Test 3	(f	1.0	0.186	20	30	572	4016	3.7	0.144	2.2
Test 4	250mm)					560	4206		0.154	
Test 5						567	3790		0.151	
Test 1						500	6553		0.263	
Test 2	0.0491					Not measured	6529		0.232	
Test 3	(f	0.54	1.502	20	30	550	6902	2.0	0.291	9.3
Test 4	250mm)					Not measured	6572		0.225	
Test 5						Not measured	6701		0.258	

Test 1						590	5053		0.236	
Test 2	0.0491					Not measured	4204		0.216	
Test 3	(*f*	0.36	0.8	20	30	Not measured	5745	11.0	0.205	5.4
Test 4	250mm)					600	4788		0.208	
Test 5						Not measured	5594		0.229	

3.1.2. Effect of surface area and nature of reflected surface

Figure 6(a) and 6(b) show a comparison of the experimentally measured reflected over pressure-time histories for the tests with aluminium skin plates (having the same mass 1.0 kg and surface roughness (0.18 µm) and different surface area (*f* 200 mm and *f* 250 mm)) with the ConWep pressure profile. Due to the limited scatter, the first three tests are shown and for the simplification, only the positive phase of the reflected pressure profile is considered. The influence of surface area on the peak reflected pressure and the corresponding positive phase duration can be understood from these figures. Although the mass of both aluminium skin plates is the same (1 kg), a 50 mm increase in diameter attributed to an increase of the average maximum reflected pressure from 3050 kPa to 4000 kPa. Subsequently, the average positive phase duration was increased from 0.12 ms to 0.145 ms. However, these values are significantly lower than the values predicted by ConWep (4755 kPa and 0.5321ms). Furthermore, Figure 6(c) and 6(d) show the reflected over pressure-time histories for sandwich composite skin plates with mass of 0.54 kg (*f* 250 mm) and 0.36 kg (*f* 250 mm) respectively. The peak reflected pressures from a few experiments with sandwich composite skin plates were comparable with ConWep data (Table 1). However, most of the experiments showed higher values of the peak reflected pressure than the ConWep predicted values (Figure 6(c) and 6(d)). Although the surface area of the two sandwich composite skin plates (*f* 250 mm) was the same, a significant difference in the magnitude of the peak reflected pressure was noticed consistently. The difference in average maximum reflected pressure between these two sandwich composite skin plates may be due to the nature of the reflected surface, mass of the skin plate and the non-homogeneous pressure cloud formation. The later explanations are not likely, because the chance of recording a consistent pressure with each sandwich composite skin plate would be very small. Furthermore, the magnitudes of peak pressure measured from the aluminum skin plate (*f* 250 mm) should also have indicated the same range of peak pressure magnitudes compared to the values from the sandwich composite skin plates. However, the magnitudes of pressure were lower than from the sandwich composite skin plates (Table 1). Secondly, the numerically calculated natural time period of these skin plates (9.0 ms, 4.09 ms and 5.021 ms for aluminium (*f* 250mm;1.0 kg) and sandwich composite skin plates respectively) is much higher than from the positive phase duration of the blast. So according to the general blast load regime [17, 18] these skin plates will be subjected to impulsive loading. Therefore, the influence of the mass of the skin plate on the peak reflected pressure can be eliminated. Hence, it can be stated that the surface roughness of the reflected surface plays a significant role for the blast parameters. The surface roughness was measured at different locations of the reflected surfaces and the average is reported here. The average maximum reflected pressure of 6650 kPa corresponds to a sandwich composite skin plate (*f* 250 mm; 0.54 kg) reflected surface with an arithmetic average surface roughness of 1.502 µm. The average maximum reflected pressure 5076 kPa corresponds to a sandwich composite skin plate (*f* 250 mm; 0.36 kg) reflected surface with the arithmetic average surface roughness of 0.8 µm. Similarly, the average maximum reflected pressure 4000 kPa corresponds to the aluminium skin plate (*f* 250 mm) reflected surface with the arithmetic average surface roughness of 0.186 µm. Furthermore, the influence of surface roughness can be observed from the positive

phase duration values. The average values of the positive phase duration were 0.25 ms and 0.21 ms for the sandwich composite skin plates (*f* 250 mm) with surface roughness of 1.502 µm and 0.8 µm respectively. Due to a smooth surface the positive phase duration of the aluminium skin plate with 250 mm diameter (0.145 ms) was lower than for the sandwich composite skin plates. These values indicate that the interaction period of the pressure waves increases with rough surface structures.

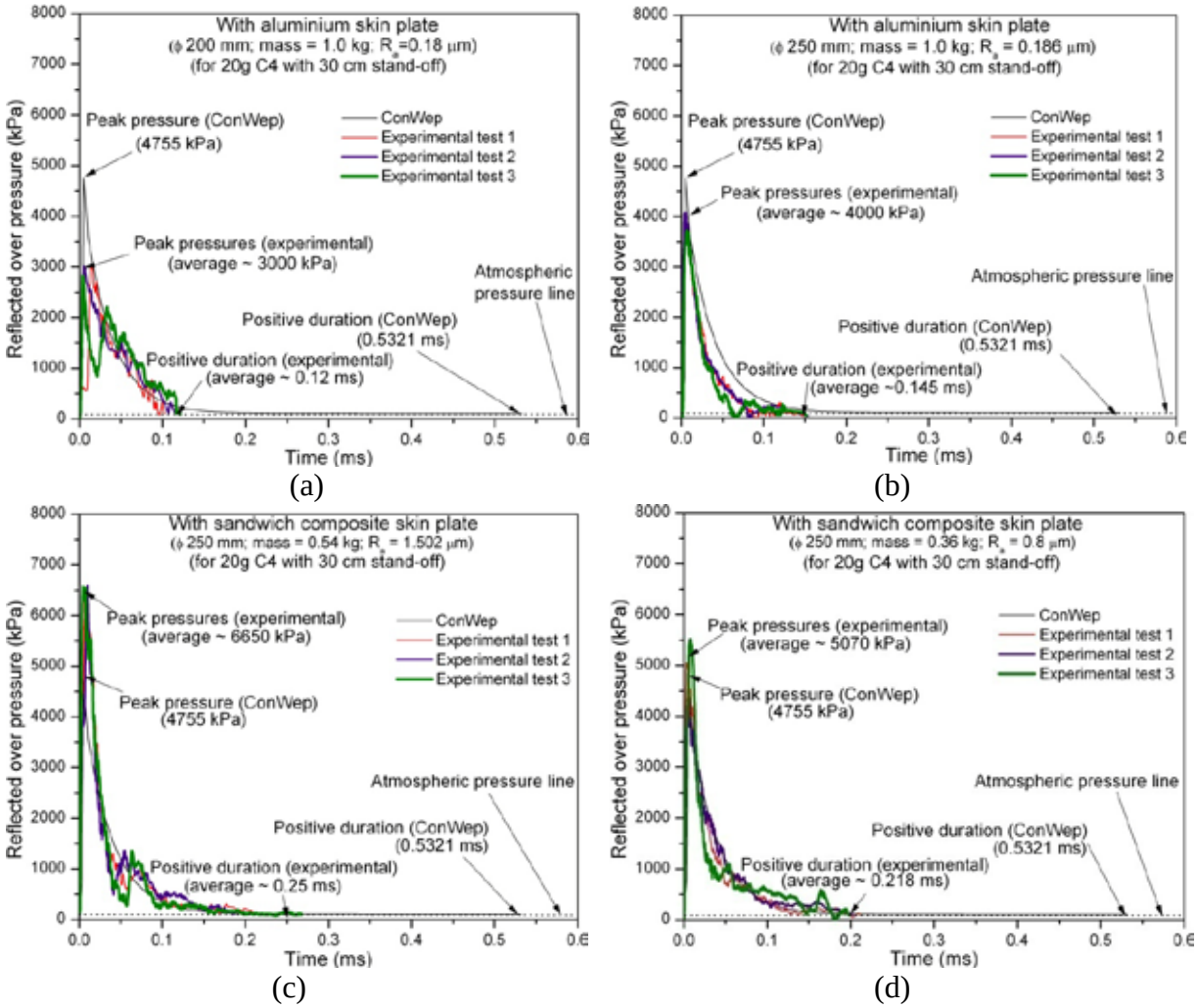

Figure 6: Comparison of experimentally measured pressure-time histories with ConWep data for 20g of C4 with a stand-off distance of 30 cm: **(a)** with aluminium skin plate (*f* 200 mm; 1.0 kg of mass; R_a = 0.18 µm). **(b)** with aluminium skin plate (*f* 250 mm; 1.0 kg of mass; R_a = 0.186 µm) **(c)** with sandwich composite skin plate (*f* 250 mm; 0.54 kg of mass; R_a = 1.502 µm). **(d)** with sandwich composite skin plate (*f* 250 mm; 0.36 kg of mass; R_a = 0.8 µm).

3.1.3. Effect of clearing phenomenon on the equivalent load

Figure 7 shows one of the experimental recordings of reflected pressure-time profile measured with sandwich composite skin plate (*f* 250 mm; mass = 0.36 kg; R_a = 0.8 µm). The peak reflected pressure magnitude (4788 kPa) of this test (refer test 4 from Table 1) was very close to the ConWep value (4755 kPa). The equivalent triangular impulse load (area below the reflected pressure curve) for the experimental curve is shown in solid line (Figure 7). This equivalent triangular impulse load was calculated based on the diffracting (engulfing) load case [18]. The approximate new positive duration for this equivalent triangular impulse load

is 0.069 ms. Next, the equivalent triangular impulse load calculated from the predicted reflected pressure-time history from ConWep is also shown in the same figure (dashed-line). The difference between these two load cases is indicated by the 45° inclined lines. The equivalent triangular impulse load from ConWep accumulates a higher amount of energy compared to the experimental curve. The reason for the significant difference between these two load cases is due to a considerable difference in positive duration. The measured and ConWep predicted positive phase duration of this case were 0.2081 ms and 0.5321 ms respectively. Considering the ConWep predicted load for this case definitely will over predict the efficiency of the core structure. Hence, the effect of clearing has to be taken into account for the correct efficiency calculation of core structures. The above discussion is valid for other skin plate cases also. Furthermore, the calculation of clearing time (the time at which the reflected pressure becomes equivalent to the incident pressure) using the standard relation may not yield the correct value for such a close-range blast loading application with finite surface area. The approximate clearing time can be calculated using the following relation [17].

$$t_c = 3 \times S / U_s \qquad (2)$$

where "*S*" is the smallest distance at which the pressure wave can pass around the edges; "U_s" is the blast front velocity. Taking "*S*" as the radius of the skin plate (100 mm and 125 mm) and assuming the value of "U_s" is approximately 440 m/s [17], the calculated clearing time was 0.68 ms and 0.85 ms for *f* 200 mm and *f* 250 mm skin plates respectively. The calculated clearing time was significantly higher than the positive duration of the blast (refer Table 1) which is physically impossible (refer Figure 6 and 7).

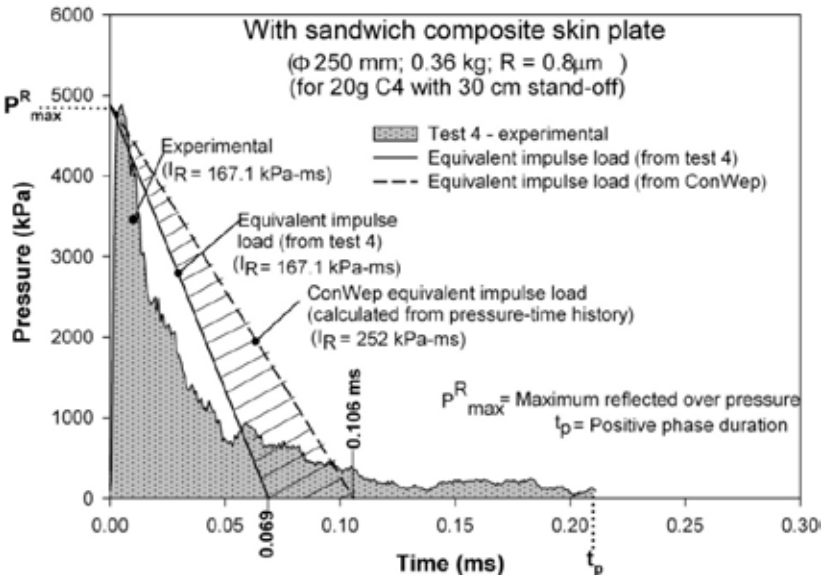

Figure 7: Effect of clearing phenomenon on the equivalent triangular impulse load (comparison of experimental and ConWep values).

3.2. Deformation pattern

The deformation patterns of the empty beverage cans from different blast tests with different skin plates are shown in Figure 8(a-d). These cans are painted after the test due to the intellectual property rights. Based on the thickness distribution of an empty beverage can, it can be concluded that the initial deformation should occur at the mid-wall location (belly

portion) of the can due to its lower thickness. However, the initial deformation of the beverage can with aluminium skin plate (f 200 mm; 1.0 kg) occurred at different points of the can along its length (refer Figure 8(a)). The difference in the deformation pattern of the cans may be influenced by a combination of two effects: (i) the initial geometry imperfections induced during the manufacturing process and during usage and (ii) a lower impact velocity of the skin plate (refer Figure 11 (b)). Due to the very small thickness at the mid-wall location (0.07 mm), plastic local wall buckling and folding occurred at different points along the length of each empty can. The average deformation length of the beverage can for this case was 8.9 mm. However, the deformation initiation of the remaining skin plates is different from the previous case (refer Figure 8(b-d)). The initial deformation started below the top shoulder region. Consequently, the deformation propagated downwards along its length. This may be due to a higher impact velocity of the skin plate and the lower thickness reduction at that location. The longitudinal cut-section of these specimens showed a clear evidence of forming lobes. The formation of lobes was uniform for the test specimens which were subjected to co-axial loading (longitudinal axis of test specimen and skin plate was aligned) during the blast event. For a few cases, there was an offset noticed between the skin plate and the test specimen during the pressure loading. Due to this effect the crushing of the cans was not uniform around their circumference and a few bigger lobes were formed on one side of can. This phenomenon can be noticed from the third test specimen shown in Figure 9(c). The average deformation length of the beverage can was 45 mm and 60 mm with sandwich composite skin plate mass of 0.54 kg and 0.36 kg respectively. Compared to the thickness of a blank can the thickness of the aesthetic coating on the outer surface and lacquer coating (used to prevent the contact of beverage with metal) at the inner surface was negligible. Hence, there was no significant effect on the deformation from these coatings. However, a detailed study is needed for the final conclusion of this statement.

(a)

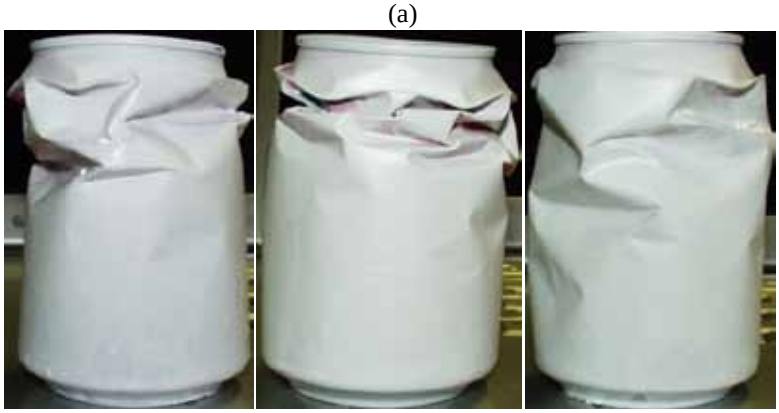

(b)

(c)

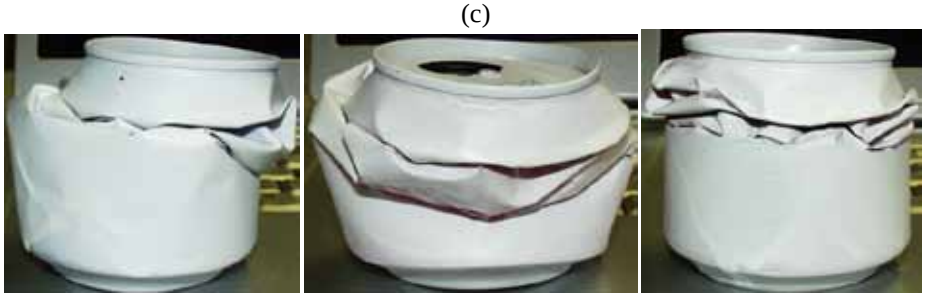

(d)

Figure 8: Deformation patterns of empty beverage cans. **(a)** with aluminium skin plate (f 200 mm; 1.0 kg of mass; R_a = 0.18 µm). **(b)** with aluminium skin plate (f 250 mm; 1.0 kg of mass; R_a = 0.186 µm). **(c)** with sandwich composite skin plate (f 250 mm; 0.54 kg of mass; R_a = 1.502 µm). **(d)** with sandwich composite skin plate (f 250 mm; 0.36 kg of mass; R_a = 0.8 µm).

3.3. Load-deformation curves

A preliminary quasi-static study of the empty beverage cans clearly indicated the strain-rate dependency on their material deformation and their peak crush load [19]. The peak crush load of an empty beverage can varied from 1.1 to 1.4 kN for 0.002 to 0.037 sec^{-1} rate of loading. As an example, the quasi-static load-deformation curve of an empty beverage can at different (low) strain rates is shown in Figure 9. For the simplification the crushing compressive load and the deformation length are shown in positive values in all load-deformation graphs.

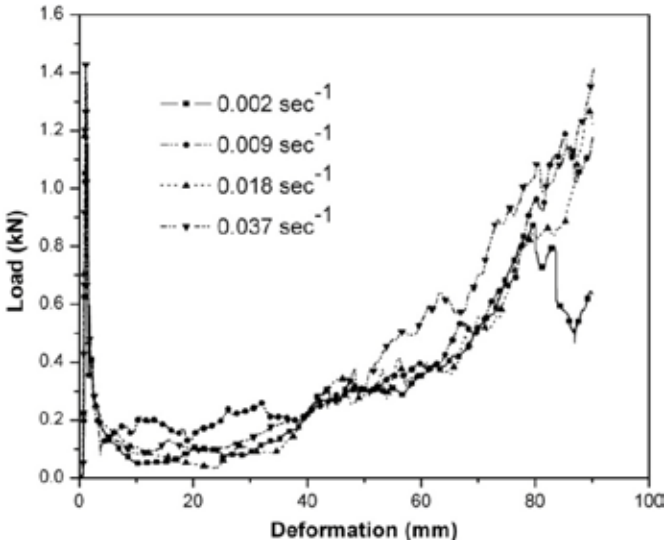

Figure 9: Quasi-static load-deformation curves of empty beverage cans at different low strain rates.

The measured load-deformation curves for the first three blast tests for different skin plates are shown in Figure 10. It was assumed that the vertical displacement of the skin plate was equivalent to the deformation length of the test specimen. The measured signal from the

accelerometer was integrated twice to get the displacement of the skin plates. From the load-deformation curves of successive tests, it can be noticed that the peak crushing load of an empty beverage can varied from 3 to 3.3 kN with aluminium skin plates (Figure 10(a) and (b)). For sandwich composite skin plate this value varied from 4.48 and 4.104 kN (refer Figure 10(c) and (d)). This value shows a clear evidence of strain-rate dependency. The total energy absorption of each test specimen during the blast event was calculated based on the following equation (3),

$$E_{abs} = \int_0^{l_{max}} F(l) \times dl \ \text{[J]} \tag{3}$$

where *F(l)* is the instantaneous crushing load corresponding to the instantaneous crushing deformation length of the beverage can *dl*. l_{max} is the maximum or total deformation length of the test specimen. The mean crushing load of the test specimen oscillated from a minimum of 0.4 kN to a maximum of 0.75 kN with different top skin plates. The mean crushing load was calculated by the following equation,

$$F_{mean} = \frac{\int_0^{l_{max}} F(l) \times dl}{l_{max}} \ \text{[kN]} \tag{4}$$

The mean crush load of the test specimen with 0.54 kg mass of the skin plate varied from a minimum of 0.523 kN to a maximum of 0.712 kN. However, the mean crush load of test specimens with 0.36 kg mass of skin plate showed consistent values (more than 0.7 kN) which is a good indicator for better energy absorption than the other cases [13]. The calculated crushing efficiency (the ratio of the mean crush load to the peak crush load which indicates the efficiency of the crushing (η_c)) of all tests is given in Table 2. The summary of test specimen crushing parameters (peak crush load, mean crush load and the energy absorption) for all cases is given in Table 2. To understand the energy absorption efficiency of each test specimen, the specific energy absorption (SEA - normalized with respect to mass) was calculated based on Equation 5.

$$SEA = \frac{\int_0^{l_{max}} F(l) \times dl}{m_e} \ \text{[J/g]} \tag{5}$$

where m_e is the mass of an empty beverage can (26 g). The test specimens which were tested with higher skin plate mass exhibited a lower SEA. The average SEA of test specimens which were tested with aluminium skin plates was 0.148 kJ/kg and 0.317 kJ/kg for 200 mm and 250 mm diameter respectively. Empty beverage cans tested with the sandwich composite skin plate showed higher values. The average values of SEA were 1.007 and 1.6604 kJ/kg for test specimens with 0.54 and 0.36 kg of skin plates respectively (refer Table 2).

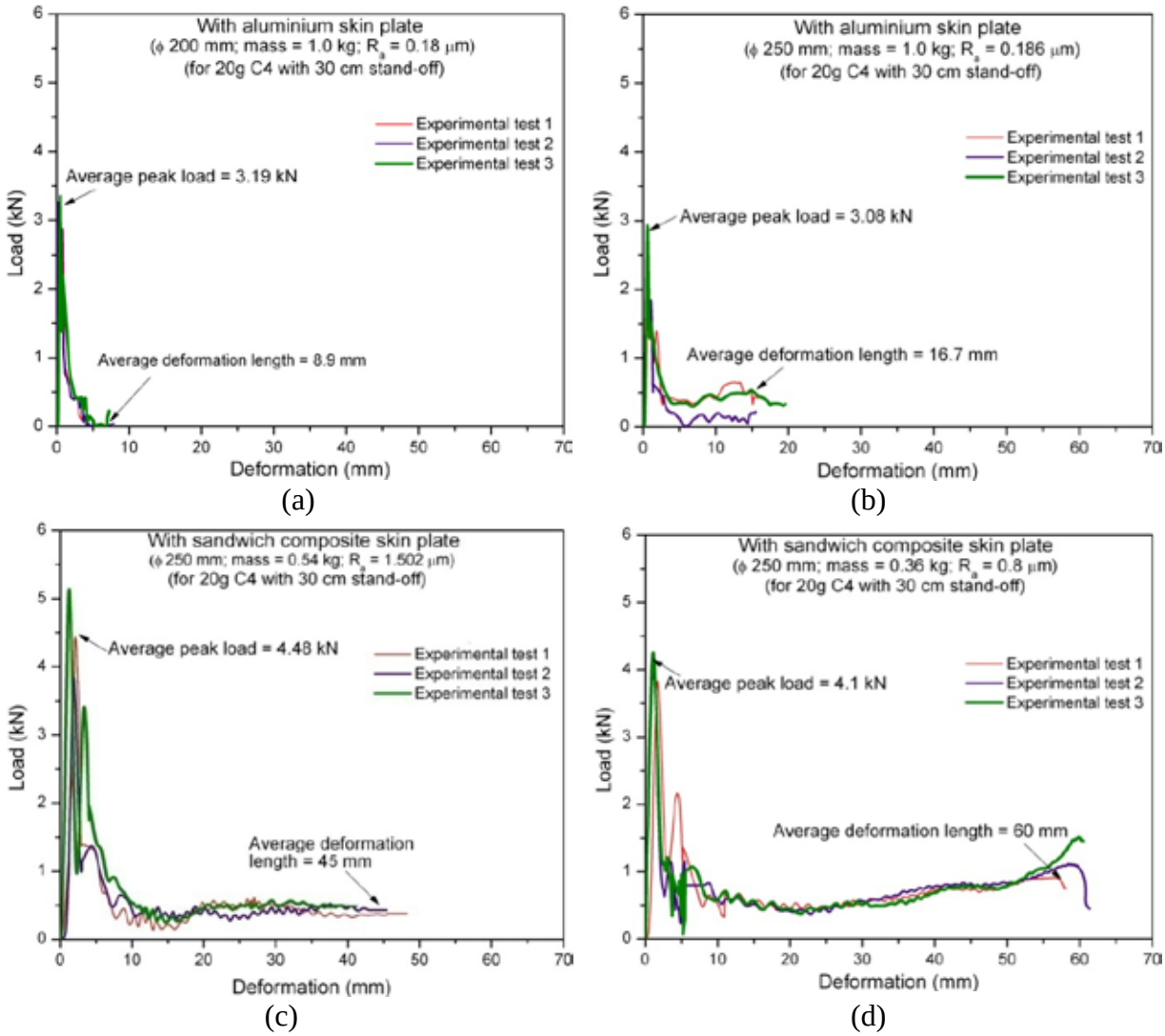

Figure 10: Force-deformation histories of beverage cans **(a)** with aluminium skin plate (ϕ 200 mm; 1.0 kg of mass; R_a = 0.18 μm). **(b)** with aluminium skin plate (ϕ 250 mm; 1.0 kg of mass; R_a = 0.186 μm). **(c)** with sandwich composite skin plate (ϕ 250 mm; 0.54 kg of mass; R_a = 1.502 μm). **(d)** with sandwich composite skin plate (ϕ 250 mm; 0.36 kg of mass; R_a = 0.8 μm).

Table 2: Summary of crushing parameters.

Test No	Reflected (total) impulse delivered to the skin plate (I_{refl})	Impulse transferred to non-sacrificial structure(I_{trans})	% difference in impulse (ΔI)	Available energy to the skin plate for beverage can crushing (E_{trans})	Energy absorbed by the beverage can (E_{abs})	Peak (crush) load (F_{max})	Mean crush load (F_{mean})	Deformation length of test specimen (l_{max})	Crush efficiency η_d	SEA
	kN-s	kN-s	%	J	J	kN	kN	mm	(%)	(kJ/kg)
With aluminium top skin plate (ϕ 200 mm; m_p= 1.0 kg; R_a= 0.18μm;)										
Reference test	0.00385	0.00258	33	-	-	12.32	-	-	-	-
Test 1	0.00392	0.00266	32	7.54	3.84	2.98	0.443	8.67	14.9	0.148
Test 2	0.00381	0.00251	34	7.07	3.32	3.34	0.403	8.23	12.1	0.127
Test 3	0.00404	0.00286	29	8.03	4.01	3.40	0.501	8.00	14.7	0.154
Test 4	0.00393	0.00263	33	7.47	3.95	2.95	0.394	10.03	13.4	0.152
Test 5	0.00400	0.00288	28	7.87	4.16	3.28	0.428	9.71	13.0	0.160
With aluminium skin plate (ϕ 250 mm; m_p= 1.0 kg; R_a= 0.186μm)										

Reference test	0.00478	0.0032	32	-	-	16.97	-	-	-	-
Test 1	0.00451	0.0029	35	11.10	8.75	2.92	0.47	15.80	18.8	0.336
Test 2	0.00516	0.0031	39	13.23	7.78	2.94	0.48	16.32	16.3	0.299
Test 3	0.00532	0.0034	36	14.02	8.66	3.01	0.44	19.60	14.6	0.333
Test 4	0.00430	0.0028	34	13.67	8.80	3.30	0.54	16.20	16.3	0.338
Test 5	0.00481	0.0030	37	11.49	7.35	3.23	0.46	15.89	14.2	0.282
With sandwich composite skin plate (f 250 mm; m_p= 0.54 kg; R_a= 1.502µm)										
Reference test	0.00912	0.00637	30	-	-	7.25	-	-	-	-
Test 1	0.01032	0.00756	27	92.89	25.94	4.44	0.533	48.7	12.0	0.998
Test 2	0.00954	0.00656	31	82.50	24.47	3.83	0.539	45.4	14.0	0.941
Test 3	0.01020	0.00629	38	92.36	29.35	5.13	0.712	41.2	13.9	1.129
Test 4	0.00976	0.00673	31	84.78	25.00	4.62	0.610	41.0	13.2	0.962
Test 5	0.01079	0.00640	40	102.1	26.14	4.39	0.523	50.0	11.9	1.005
With sandwich composite skin plate (f 250 mm; m_p= 0.36 kg; R_a= 0.8µm)										
Reference test	0.00879	0.00633	28	-	-	6.01	-	-	-	-
Test 1	0.00823	0.00592	28	90.8	41.96	3.95	0.723	58.0	18.3	1.614
Test 2	0.00870	0.00629	27	102.1	44.49	4.48	0.723	61.5	16.1	1.711
Test 3	0.00845	0.00657	22	92.3	45.42	4.25	0.750	60.5	17.6	1.746
Test 4	0.00864	0.00625	28	97.6	40.01	4.01	0.702	57.0	17.5	1.539
Test 5	0.00901	0.00635	30	106.2	43.98	3.83	0.709	62.0	18.5	1.692

3.4. Effect of skin plate inertia

The efficiency of the energy absorption of the inner core will be reduced if the skin plate interacts with the blast pressure over significant duration of the blast time. Furthermore, the inertia of the skin plate is another parameter which controls the amount of energy transferred to the inner core. A significant amount of blast energy has to be spent on the skin plate if the inertia of the skin plate is larger. Hence, a comparison was made for three skin plates (one aluminium skin plate and two sandwich composite skin plates) having the same surface area (f 250 m). The available energy for the crushing of the beverage can (or) the energy transmitted from the blast wave to the skin plate was calculated based on the following relation (Equation 6).

$$E_{trans}(t) = \int_0^{t_p} p(t) \times A_p \times v(t) \times dt \quad [\mathrm{J}] \tag{6}$$

where A_p is the area of the skin plate; $v(t)$ is the velocity of the top skin plate in m/s (integrated acceleration signal measured from the skin plate during the experimental test). Figure 11(a) shows the available energy to the skin plate for the crushing. It is very clear that a significant amount of energy has been spent to overcome the inertia of the skin plates. The average energy given by the sandwich composite skin plates was 90 J and 97 J for 0.54 kg and 0.36 kg respectively. However, the energy delivered by the aluminium skin plate (f 250 mm; 1.0 kg of mass; R_a = 0.186 µm) was much lower (12.5 J) than for the sandwich composite skin plates. The maximum attained velocity of the skin plates depends on the peak reflected pressure and the mass of the skin plate. A higher peak pressure and a lower mass of the skin plate will provide a higher attained velocity of the skin plates which has an influence on the crushing response of the test specimens. As a result, the maximum velocity attained by the aluminium skin plate was lower than for the other two cases (refer Figure 11(b)). Due to the different levels of the attained velocity of the skin plates, a significant difference in the

deformation length (integrated twice from the acceleration signal) of the test specimens was noticed. The average maximum deformation length achieved with the aluminium skin plate (f 250 mm; 1.0 kg of mass; R_a = 0.186 µm) was 16.7 mm. Skin plates with lower masses attributed to a higher crushing length of the test specimens. The sandwich composite plate with 0.54 kg yielded an average deformation length of 45.25 mm. Similarly, the sandwich composite skin plate with 0.36 kg provided an average deformation length of 60 mm (refer Figure 11(b) and Figure 8(c-d)).

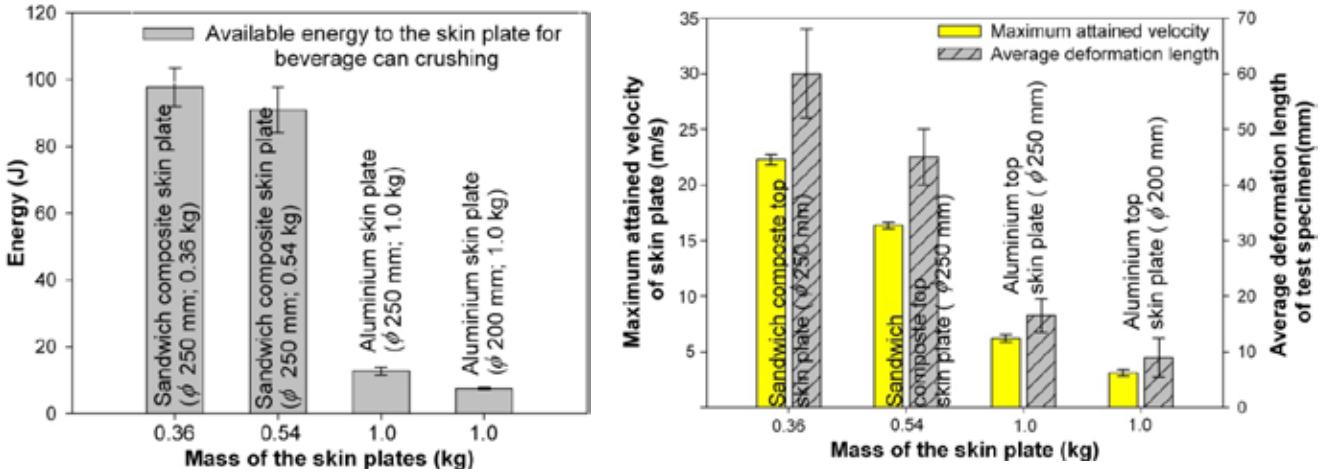

(a) (b)

Figure 11: (a) Effect of inertia of skin plate on the available energy to the skin plate for beverage can crushing (error bar indicates the standard deviation). **(b)** Effect of inertia of skin plate on the maximum attained velocity of skin plate and the corresponding deformation length achieved by the beverage cans (error bar indicates the standard deviation).

3.5. Impulse and energy transfer

In order to understand the effectiveness of the empty beverage can the impulse delivered to the top face of the skin plate (reflected impulse) and the corresponding transferred impulse at the bottom of the beverage can to the non-sacrificial member (integration of measured force-time history at the bottom of the beverage can) are compared. The reflected impulse and the transferred impulse were calculated based on the following relations (Equation 7 and 8)

$$I_{refl} = \int_0^{t_p} p(t) \times A_p \times dt \quad \text{[kN-s]} \tag{7}$$

$$I_{trans} = \int_0^{t} F(t) \times dt \quad \text{[kN-s]} \tag{8}$$

where $F(t)$ is the measured reaction force at the bottom of the beverage can. Similarly, the energy transmitted by the blast wave to the skin plate and the corresponding energy absorbed by the beverage cans were calculated using Equations 6 and 3 respectively. The calculated values of I_{refl} and I_{trans} for all cases are given in Table 2. It can be observed that the linear momentum is not conserved for any of the cases. One of the reasons might be the recording of the transferred force signal for a shorter duration compared to the complete event of beverage can crush. However, even after increasing the recording duration significantly, the same difference was observed for all cases. The difference between the reflected impulse and the transferred impulse for all cases is given in Table 2. This result is unexpected, because

any sacrificial cladding structure cannot prevent the impulse of the blast being transferred onto the structure upon which it is mounted, rather it changes the force-time distribution from a high load, short duration impulse to a low load, long duration impulse and thereby avoiding or reducing the damage to the non-sacrificial structure upon which it is mounted. As an example, one of the cases with sandwich composite skin plate (ϕ 250 mm; 0.54 kg of mass; R_a = 0.8 µm) is presented here. The applied load and the corresponding reflected impulse given to the top face of the sandwich composite skin plate are shown in Figure 12(a); and the corresponding transferred load and impulse to the non-sacrificial structure are shown in Figure 12(c). Furthermore, the peak load from the reference test (average of two tests conducted without test specimen and only with skin plate directly placed on the dynamic load cell for the same loading parameters (20 g C4 with 30 cm stand-off distance)) is also given in Table 2. It can be noticed that the use of the beverage can reduced the peak load from 7.25 kN to about 4 kN considerably and the corresponding positive duration was extended significantly (11.8 ms – refer Figure 12(c)). However, the same figures (Figure 12(a) and (c)) also show the difference in the impulses. Similarly, there was a significant difference noticed between the available energy to the skin plate for beverage can crushing (90.8 J) and the corresponding energy absorbed by the beverage can (refer Figure 12(b), Figure 12(d) and Table 2). If we assume, the difference might be due to the energy absorbed by the top skin plate; then one can expect a significant deformation of the skin plates during the experiments. However, there was no significant deformation observed during these tests. Hence, the question of why such a difference occurs for both impulse and the energy is to be answered. For that the complete knowledge of interaction of pressure waves with the test set-up and the corresponding effects are to be captured in detail. Hence, coupled blast simulations were carried out using Hydrocodes (Autodyn V-11.0) with two different skin plates (aluminum and sandwich composite). The details of the modelling and the corresponding results are presented in next section.

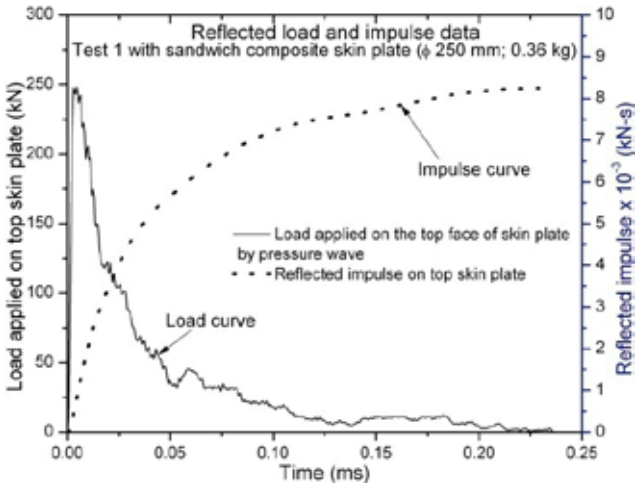

(a)

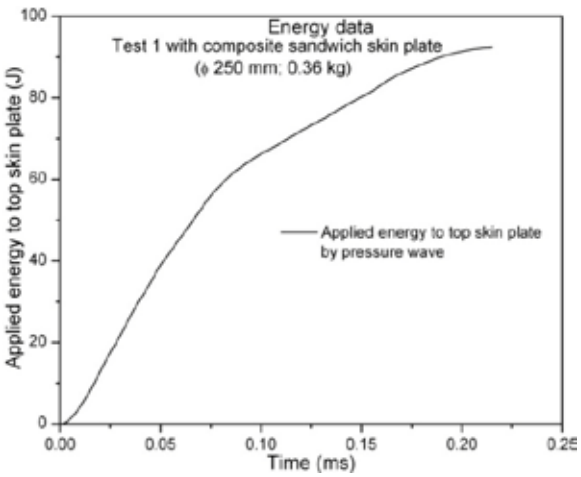

(b)

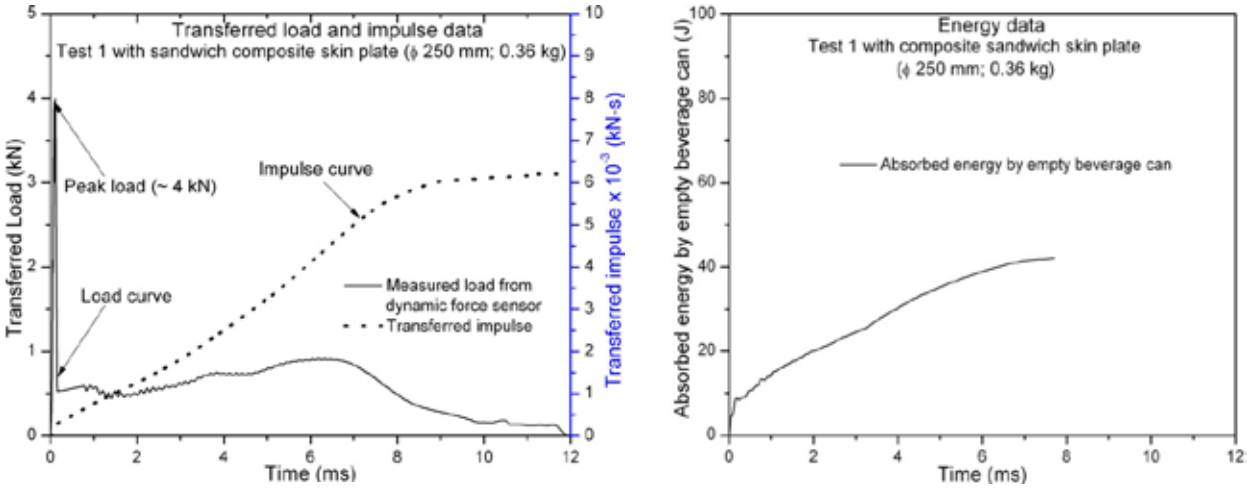

Figure 12: (a) Reflected impulse (load-time history) of sandwich composite skin plate (*f* 250 mm; 0.54 kg of mass; R_a = 0.8 µm) **(b):** Energy delivered by the reflected pressure wave to the sandwich composite skin plate (*f* 250 mm; 1.0 kg). **(c):** Transferred impulse (load-time history) to the non-sacrificial structure due to the beverage can crushing. **(d)**: Energy absorbed due to the crushing of beverage can.

4. Numerical simulation of blast loading

The predicted peak reflected pressure and its positive duration from the aluminium skin plate were significantly lower than from the ConWep values. On the contrast, for most of the cases the peak reflected pressure from the sandwich composite skin plates was higher than from the ConWep predicted values. Hence, to understand the behaviour of these skin plates during blast loading, both skin plates (aluminium skin plate with *f* 200 mm and 1.0 kg; sandwich composite skin plate with *f* 250 mm and 0.54 kg) have been chosen for the numerical study. The commercial tool Autodyn V-11.0 was used to carry out the blast pressure interaction simulation for the discussed experimental set-up. In order to reduce the computational time the blast simulation for the discussed experimental set-up was done in two stages. The first stage is the analysis of initiation of the explosion of C4 from the detonation point and propagation of the pressure waves. In Autodyn V-11.0 this analysis can be done using 2D approach. The second part deals with the propagation and interaction of blast pressure with the test set-up in a 3D computational model using 2D data. The remapping option of Autodyn provides this feature. With the help of developed computational models the interaction of blast pressure wave with the test set-up is clearly captured. Furthermore, the question of why the total reflected impulse is not transferred to the non-sacrificial structure is also answered.

4.1. 2D Blast simulation

The unique capability of remapping of Autodyn greatly reduced the number of grids or elements to achieve accurate blast parameters [20]. In order to study the detonation of the C4 explosive a wedge model was used (Figure 13). Accordingly 1000 grids (elements) were chosen along the "Y" axis in the air medium. The air and C4 were modelled using multi-material Euler formulation. The initiation, detonation and the expansion of C4 was modelled using the Jones-Wilkins-Lee (JWL) Equation of state (EOS) (refer Table 3 for details). The spherical charge of 20g C4 was modelled with an equivalent radius of 14 mm in the 2D model. Similarly, the wedge area filled with ambient air was modelled using the ideal gas EOS (Table 3). The length of the wedge model was 30 cm. Using this model, the incident

pressure-time history at a distance of 30 cm from the centre of detonation of C4 was calculated. The contours of the simulated incident pressure at 30 cm from the detonation centre are shown in Figure 13. These symmetric (about the "Y" axis) spherical data were written into a remap file and then imported into a 3D air model.

Table 3: Details of used Equation Of States and the corresponding material models.

S.No	Name of the part	EOS used	Equation and used parameters
1.	Air medium	Ideal gas	$p = (\gamma - 1)\rho e$ p = hydrostatic pressure; ρ = 1.225 kg/m^3; adiabatic gas constant γ = 1.4; e = 2.068 x 10^5 kJ/kg [21]) $\gamma = \omega + 1$ ω is the adiabatic constant of explosive material
2.	Explosive (C4)	JWL	$p = C_1\left(1 - \frac{\omega}{r_1 u}\right)\exp^{-r_1 u} + C_2\left(1 - \frac{\omega}{r_2 u}\right)\exp^{-r_2 u} + \frac{\omega e}{u}$ (p – hydrostatic pressure; ρ is the density [kg/m^3]; $u = 1/\rho$ is the specific volume [m^3/kg]; adiabatic constants C_1 = 6.097699 x 10^8 kPa; C_2 = 1.2950 x 10^7 kPa; r_1 = 4.5; r_2 = 1.4 and ω = 0.25; the ratio of the current volume to the original volume of the explosive material reaches more than 10, then the EOS changed to ideal gas)
3.	Aluminium skin plate	Mie-Gruneisen	$p = p_H + \Gamma_\rho (e - e_H)$ (e = energy (J); Γ_ρ = constant; p_H and e_H are variables) $\Gamma_\rho = \Gamma_0 \rho_0$ $p_H = \frac{\rho_0 C_0^2 \mu(1+\mu)}{[1-(S-1)\mu]^2}$ $e_H = \frac{1}{2}\frac{p_H}{\rho_0}\left(1 + \frac{\mu}{1+\mu}\right)$ ρ_0 is the initial density [kg/m^3]; Γ_0 is the Gruneisen coefficient [21]; $\mu = \frac{\rho}{\rho_0} - 1$; C_0 (m/s)
4.	Metal beverage can	Linear	$p = K\mu$ K is the bulk modulus of the material
5.	Glass-epoxy composite plates	Orthotropic with shock effect	$\Delta p = p_r(e_{vol}) + \frac{\Gamma(u)}{u}[e_r - e_r(e_{vol})] - \frac{1}{3}[C_{11}+C_{12}+C_{13}]\Delta e_{11}^d - \frac{1}{3}[C_{21}+C_{22}+C_{23}]\Delta e_{22}^d - \frac{1}{3}[C_{31}+C_{32}+C_{33}]\Delta e_{33}^d$ $p_r(e_{vol})$ and $e_r(e_{vol})$ define the material pressure, volume and energy relationship following the Hugoniot shock reference curve; The Gruneisen gamma $\Gamma(u)$ allows extrapolation to material state of the reference curve and is a thermodynamic property of the material; C_{ij} = material constants [21].
6.	Polyurethane foam	Linear	$p^{n+1} = p^n + K\dot{e}^{n+1/2}\Delta t^{n+1/2}$ (p = pressure; K= shear modulus; S= stress deviator; G = Bulk modulus; e = volumetric strain; Δt = incremental time; n = number of increments)
S.No	**Name of the part**	**Material model used**	**Equation and used parameters**

1.	Aluminium skin plate	Johnson-Cook	$\sigma_y = \left(A + B\bar{\varepsilon}^{p^n}\right)\left(1 + C\times \ln \dot{\varepsilon}^*\right)\left[1 - T^{*m}\right]$ $\dot{\varepsilon}^* = \dot{\bar{\varepsilon}}^p / \dot{\varepsilon}_p$ =Effective plastic strain rate $T^* = \frac{T - T_{room}}{T_{melt} - T_{room}}$ A = 265 MPa; B = 426 MPa; n=0.34; c = 0.015; m = 1.0 [22]
2.	Metal beverage can	Johnson-Cook	For body: A = 792 MPa; B = 510 MPa; n=0.26; c = 0.014; m = 1.03 [23] For top cover: refer aluminium skin plate details
3.	Glass-epoxy	Tsai-Wu	$F_1\sigma_1 + F_2\sigma_2 + F_{11}\sigma_1^2 + F_{22}\sigma_2^2 + F_{66}\tau_{12}^2 + 2F_{12}\sigma_1\sigma_2 = 1$ $F_1 = \frac{1}{X_1^T} - \frac{1}{X_1^C}; F_{11} = \frac{1}{(X_1^T X_1^C)}; F_{22} = \frac{1}{X_2^T} - \frac{1}{X_2^C}$ $F_{22} = \frac{1}{(X_2^T X_2^C)}; F_{66} = 1/S_6^2$ $F_{12} = -\frac{1}{2}\sqrt{F_{11}F_{22}}$ Refer Table 4 for description of used symbols and their values.
4.	Polyurethane foam	Strength	Refer Figure 16 for crushing characteristics of polyurethane foam.

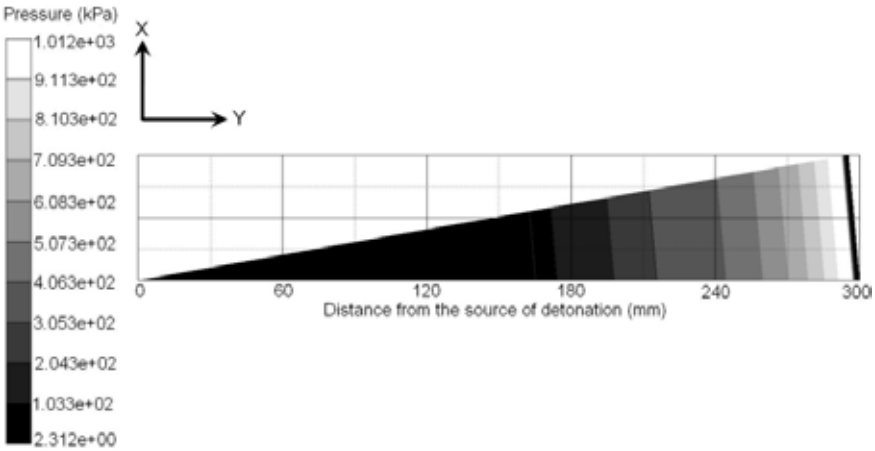

Figure 13: Wedge model (incident over-pressure contours for 20g of C4 with 30 cm stand-off distance).

4.2. 3D Blast simulation with aluminium and sandwich composite skin plate

The modelling details of 3D computational model are shown in Figure 14(a) and the corresponding EOS, material models and its data are given in Table 3. The air was modelled as a rectilinear box with Eulerian grid. The boundary of the air model was chosen to have adequate air space in all directions from the centre of detonation. The field data which were created from the 2D simulation were remapped (symmetrical about "Y" axis and 30 cm away from the top face of skin plates into the 3D air model. In order to reduce the complexity in the EOS, in addition to the skin plates the side tube was also modelled as an aluminium tube. The aluminium skin plate and the side tube were modelled by solid brick elements with eight nodes. For a close stand-off air blast loading, the air molecules at the centre of the pressure wave interact initially with the structure due to shorter distance of travelling. This central spherical wave can have a significant influence on the overall behaviour of the structure. To capture this effect, a uniform and fine mesh was introduced at the centre of the aluminium

skin plate. In order to avoid the spurious reflection of pressure wave at the interface of fine/coarse mesh [24-27], the size of the elements was increased gradually (adjacent elements size was chosen in such a way that the size ratio of these elements should not go beyond 1.5 as suggested in ref. [27]).The mesh patterns of the skin plate and the side tube are shown in Figure 14(b). Similarly, the beverage can was modelled with shell elements as per the geometry which was shown in Figure 3(a-b). In order to reduce the computation time the bottom resting plate and the copper tube were modelled as rigid bodies and subsequently, all translational and rotational degrees of freedom were arrested.

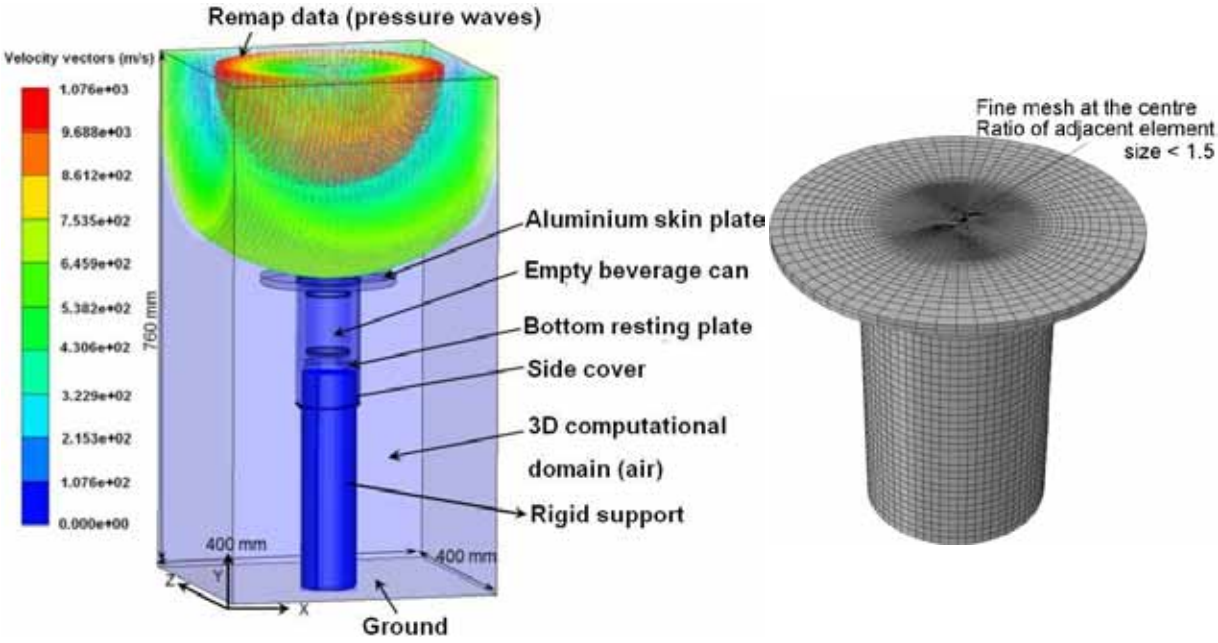

Figure 14: (a) - 3D computational model for simulating blast waves with aluminium skin plate. **(b)** - Mesh pattern of aluminium skin plate assembly.

To account the energy absorbed by the composite skin plates and the polyurethane foam the finite element modelling of the sandwich composite plate was done as per the assembly sequence which is shown in Figure 15. The top and bottom composite faces were modelled with shell elements. To capture the compression behaviour the polyurethane foam was modelled with solid 8 node brick elements. The details of EOS, used symbols and the corresponding material details are given in Table 3. The polyurethane foam strength model was represented by means of the crush characteristics (refer Figure 16).

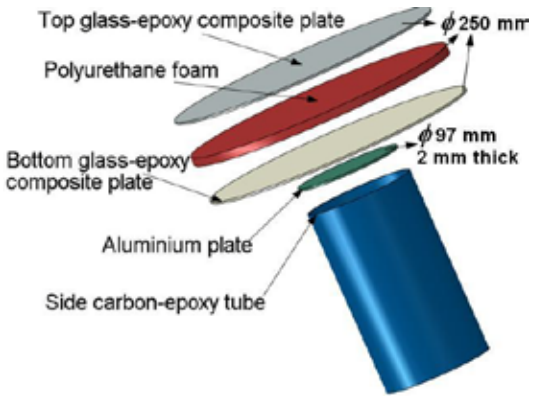

Figure 15: Assembly sequence of the sandwich composite skin plate.

Table 4: Material properties of glass epoxy composite laminates in principal directions.

Parameters	Symbol	Values
Material and elastic data		
Density (kg/m^3)	ρ	1870
Longitudinal modulus in warp direction (GPa)	E_{11}	24.25
Transverse modulus in weft direction (GPa)	E_{22}	24.25
In-plane shear modulus (GPa)	G_{12}	4.83
Poisson's ratio	v_{12}	0.153
Glass-epoxy composite Strength		
Failure criteria	-	Hashin
Tensile strength in warp (MPa)	X_1^T	390.7
Compressive strength in warp (MPa)	X_1^C	345.1
Tensile strength in weft(MPa)	X_2^T	390.7
Compressive strength in weft(MPa)	X_2^C	345.1
In-plane shear strength (MPa)	S^L	100.6

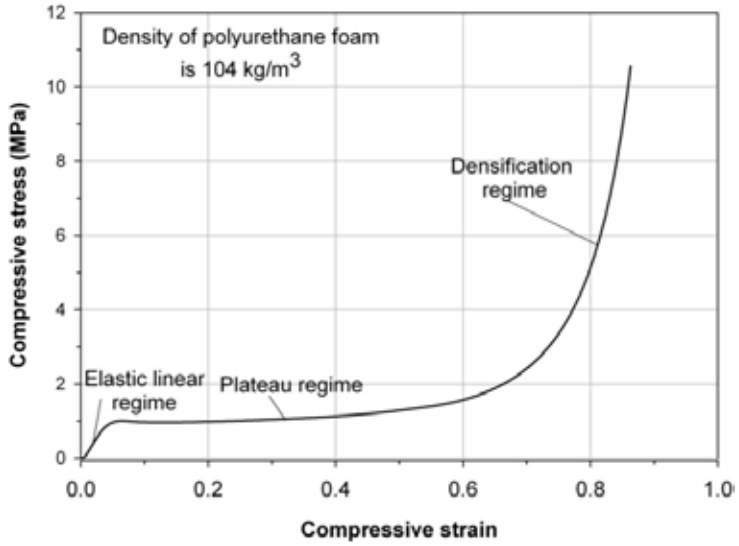

Figure 16: Crushing characteristic of polyurethane foam.

4.2.1. Applied boundary conditions and contact controls

On the rectilinear air flow domain, the "flow-out" boundary condition was assigned to all boundary planes of the 3D domain except the base plane, which represented the ground surface. This boundary condition is needed to simulate the reflection of pressure waves from the ground surface. The interaction of blast pressure waves with the skin plates and the side tube was defined by a fully coupled feature available in Autodyn V-11.0. To simulate the same experimental condition of the side tube, the translational degrees of freedom of the skin plates in "X" and "Z" directions were arrested. Similarly, the rotation of the skin plates with respect to the "Y" axis was also arrested. The bending of the skin plates with respect to "X" and "Z" axis was allowed. A "*surface-to-surface*" master-slave contact algorithm was established with a friction coefficient equal to 0.2 for two pairs. The first pair consists of the skin plate and the beverage can and the second pair consists of the bottom resting plate and the beverage can. In addition to that a self contact algorithm was also incorporated for the empty beverage can model. For sandwich composite skin plates it was assumed that the top and bottom composite faces, foam, aluminium plate (f 97 mm; 2mm thick) and the side tube are rigidly connected (refer Figure 15). Accordingly a rigid connection was established at the interfaces of all these parts.

5. Results and discussions

A blast simulation with fully coupled Lagrangian and Eulerian formulation for the empty beverage can (20g of C4 and a stand-off distance of 30 cm) was carried out. A few researchers [20, 28] have concluded that the grid size of the air model plays an important role to predict the blast parameters. In order to study the effect of the grid size on the blast parameters, a mesh sensitivity study was conducted for the air model with the aluminium skin plate (f 200 mm; 1.0 kg). The effect of grid or element size on the peak reflected pressure values can be easily understood from the Figure 17. For a smaller element size (0.25 mm and 0.5 mm) the magnitude of the peak reflected pressures (4849 kPa and 4745 kPa respectively) were very close to the ConWep value (4755 kPa). There was no significant difference in the positive duration noticed due to the change in size of the element (minimum 0.18 ms; maximum 0.183 ms). However, these values are significantly higher than the experimental values (refer Table 1). The reason for this difference is the surface roughness of the skin plates which cannot be included in the present numerical analysis. An element size of 0.25 mm was used for all the analysis.

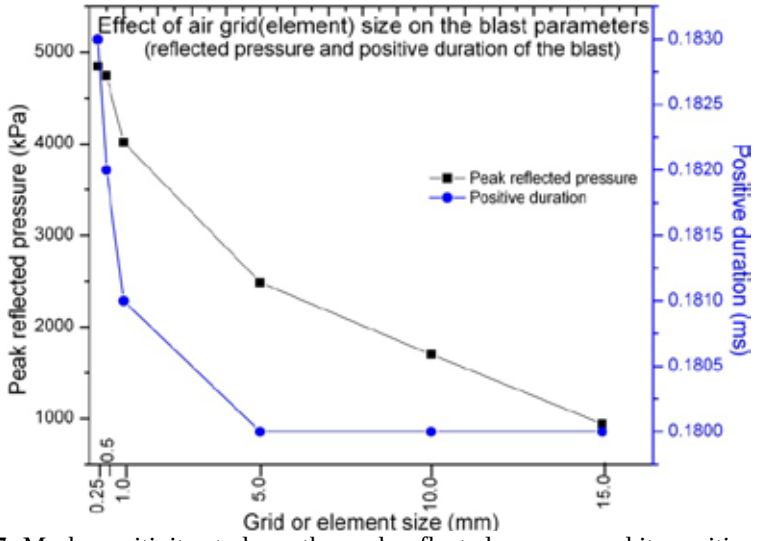

Figure 17: Mesh sensitivity study on the peak reflected pressure and its positive duration.

5.1. Interaction of blast waves and the corresponding blast parameters

After remapping the analysis was started when the pressure wave reached 1 mm above the top face of the aluminium skin plate. The magnitude of the pressure wave increased suddenly when the incident pressure was obstructed by the top face of the skin plates. This event started approximately 1.1 µs after the start of the simulation at the centre of the top face of the skin plate; and it lasted for approximately 0.01 ms. After that the amplitude reduced exponentially. During this period a significant amount of pressure waves (especially the pressure wave at the periphery of the top face of the skin plates) diffracted around the top edge of the skin plates. This shows that the wavelength of the pressure wave is greater than or equal to the diameter of the skin plates. Due to the limited surface of the skin plates the reflected pressure wave reached the edges in a very short time. This event of diffraction is called “clearing” of the reflected pressure waves. Due to this clearing the magnitude of the reflected pressure wave was reduced significantly in short time; furthermore, the diffracted pressure wave acted on the bottom face of the skin plates. As an example, the above said interaction of pressure wave for aluminum skin plate is shown in Figure 18.

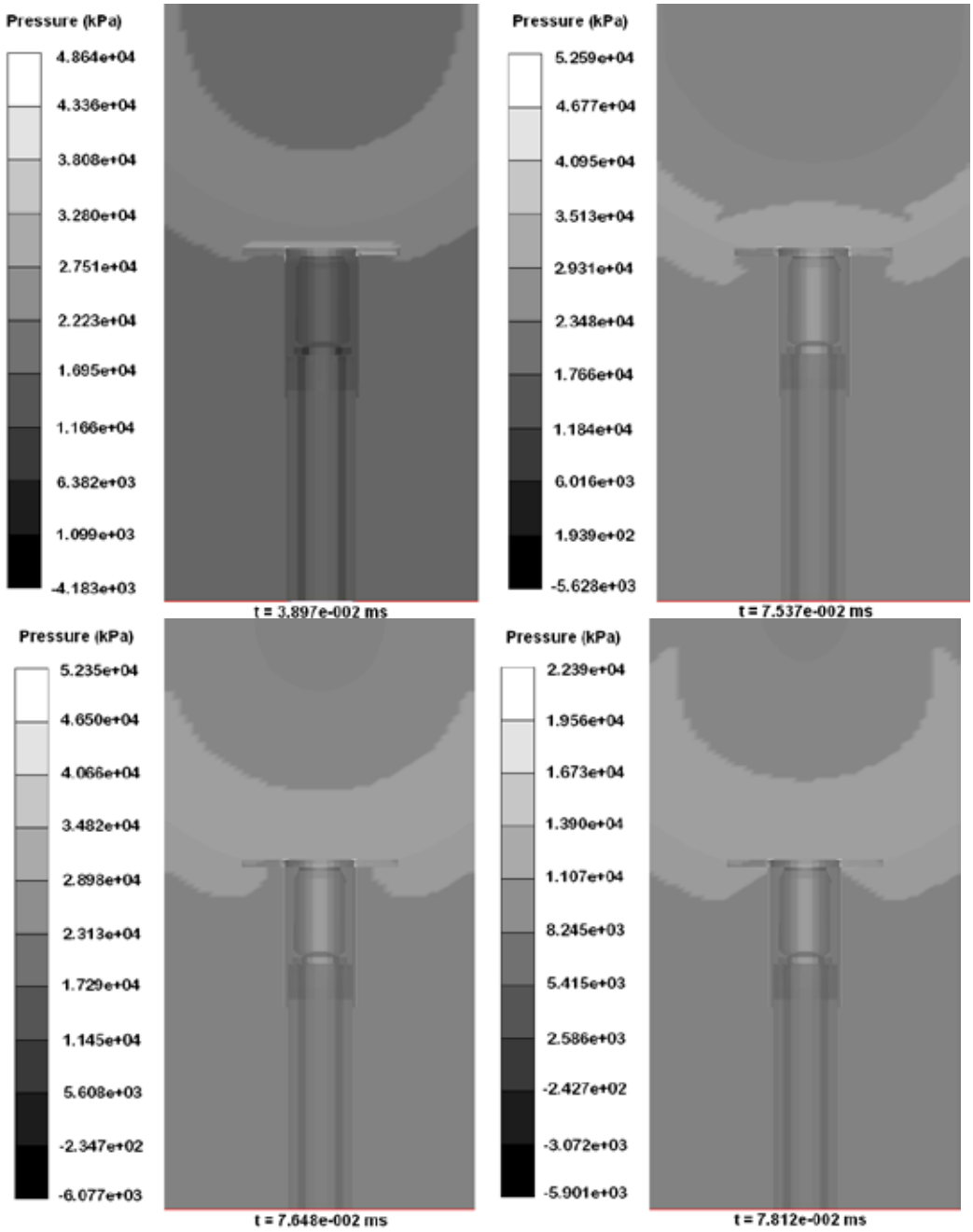

Figure 18: Interaction of blast pressure waves with the aluminium skin plate.

The calculated pressure-time history of the pressure waves at the top and bottom faces (70 mm from the centre) of the skin plates is shown in Figure 19. It can be noticed that the magnitude of the diffracted pressure and its duration at the bottom face was significant compared to the peak reflected pressure at the top face of the skin plates. The rise in pressure at the bottom face was noticed approximately 0.008 ms later than the rise in pressure at the top face of the skin plates. This was due to the time taken for the pressure waves to reach the edges and to create the subsequent diffraction phenomenon. In addition to the diffracted pressure, the direct pressure waves from the explosion at the boundary of the skin plates also contributed to increase the pressure at the bottom face of the skin plates (engulfing phenomenon). Subsequently, the magnitude of the pressure wave was exponentially reduced to the atmospheric pressure due to the undisturbed air volume below the skin plates. The calculated average impulse from the diffraction (area below the diffracted pressure curves in Figure 19) for these cases was 41.89 kPa-ms (0.0013 kN-s) and 40.82 kPa-ms (0.002 kN-s)

for the aluminium (ϕ 200mm) and sandwich composite (ϕ 250mm) skin plates respectively. In order to verify the diffraction phenomenon during the experimental testing, a few experimental tests were conducted with a high speed camera (Photron APX RS 250K capable of recording 250,000 fps). A frame rate of 10,000 fps was used for these tests. High speed images from the experiments showed a clear evidence of diffraction and subsequent pressure acting on the bottom face of the skin plates (refer Figure 20).

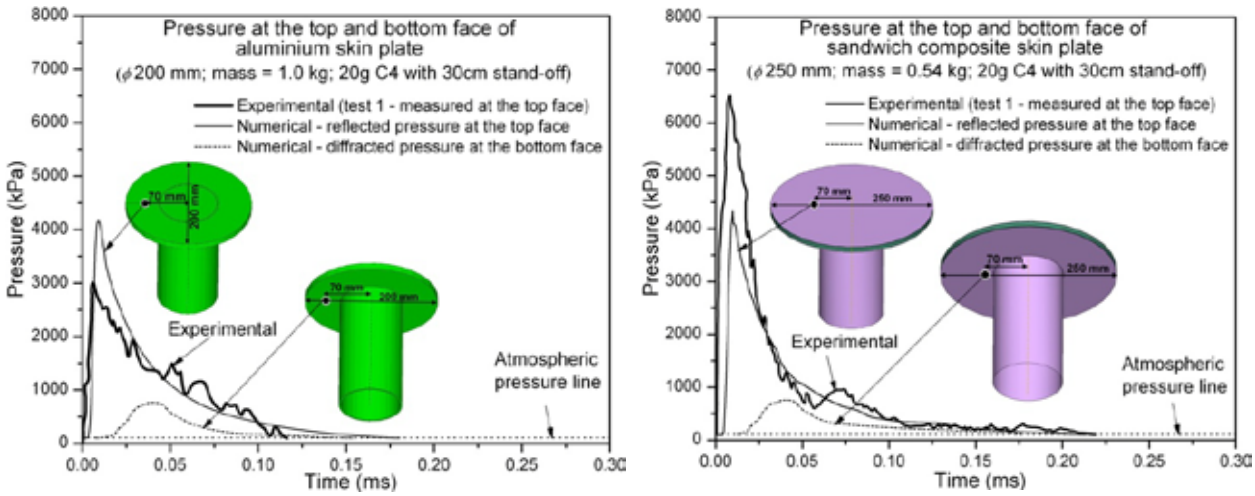

(a) (b)

Figure 19: (a) Pressure interaction at top and bottom faces of the aluminium skin plate (ϕ 200 mm; 1.0 kg). **(b)** Pressure interaction at top and bottom faces of the sandwich composite skin plate (ϕ 250 mm; 0.54 kg).

Figure 20: High speed image evidences for diffraction of blast waves during blast loading (with aluminium skin plate).

As we noticed from Figure 19(a-b) the peak reflected pressure on the top face of the skin plates from the Autodyn simulations (4849 kPa for aluminium skin plate; 4960 kPa for sandwich composite skin plate) were very close to the ConWep value (4755 kPa). On the contrast, the average positive phase duration from the numerical simulation (0.187 ms for the aluminium skin plate; 0.2089 ms for the sandwich composite skin plate) was much lower than the ConWep predicted values (0.532 ms). This difference is due to the fact that ConWep (based on empirical relations) does not take into account the finite reflected surface area. However, for the aluminium skin plate the peak reflected pressure and the positive duration values from these two approaches (ConWep and Autodyn) were higher than for the experimental data (refer Figure 6(a)). On the other hand, the peak reflected pressures for the sandwich composite skin plate from the Autodyn and ConWep (4960 kPa and 4755 kPa respectively) were lower (refer Figure 6(b)) than the experimental value (average is 6650 kPa). The reason for the significant differences in the peak reflected pressure is the surface roughness of the top face of the skin plates which cannot be included in the present numerical simulation analyses. As a result of the different peak reflected pressure, the calculated average impulse from the Autodyn simulation for the aluminium skin plate (153.7 kPa-ms (0.00482 kN-s)) was higher than the average experimental impulse (125.41 kPa-ms (0.00394 kN-s)). The calculated average impulse from the Autodyn simulation for the sandwich composite skin plate (155.7 kPa-ms (0.00764 kN-s)) was lower than the average experimental

impulse (206.2 kPa-ms (0.0101 kN-s)). Furthermore, the results from these analyses it can be concluded that the mass of the skin plate does not influence the peak reflected pressure.

At later time increments of the analysis showed an interesting phenomenon of interaction of ground reflected pressure with the skin plates. The reflection of the pressure waves at the ground surface lasted about 0.7 ms. The magnitude of the pressure wave at the ground reflection was approximately 328 kPa (Figure 21). This reflected pressure wave propagated rapidly back to the bottom face of the skin plates and during the propagation the magnitude was reduced to approximately 130 kPa. The rapid propagation of this reflected pressure wave to the skin plates might be accelerated by the negative pressure (below atmospheric pressure) below the skin plates. The reflected pressure wave from the ground acts on the bottom face of the skin plates around 1.24 ms and 1.4 ms for aluminium and sandwich composites respectively; subsequently, the diffraction of this pressure wave occurred around the edge of the skin plates (Figure 21). However, due to the lower magnitude of this diffracted pressure wave there was no significant effect observed on the top face of the skin plates. Due to the reflection phenomenon the magnitude of the pressure wave was increased to two times of its incident value (refer Figure 22). The calculated average impulse (without considering the negative impulse) due to the ground reflection was 9.23 kPa-ms (0.00029 kN-s) and 9.18 kPa-ms (0.00045 kN-s) for aluminium and sandwich composite skin plates respectively. The combined impulse from diffraction and ground reflection at the bottom face of the skin plate was approximately 33% and 30% of the total reflected impulse at the top face of aluminium (f 200 mm; 1.0 kg) and sandwich composite skin (f 250 mm; 0.54 kg) plates respectively. Now, these values can be compared with the average difference in impulse ($\Delta I = I_{refl} - I_{trans}$) observed during the experimental testing (refer Table 2). From the results of the above analyses it can be concluded that a part of the total impulse was lost due to the diffraction and ground reflection phenomena.

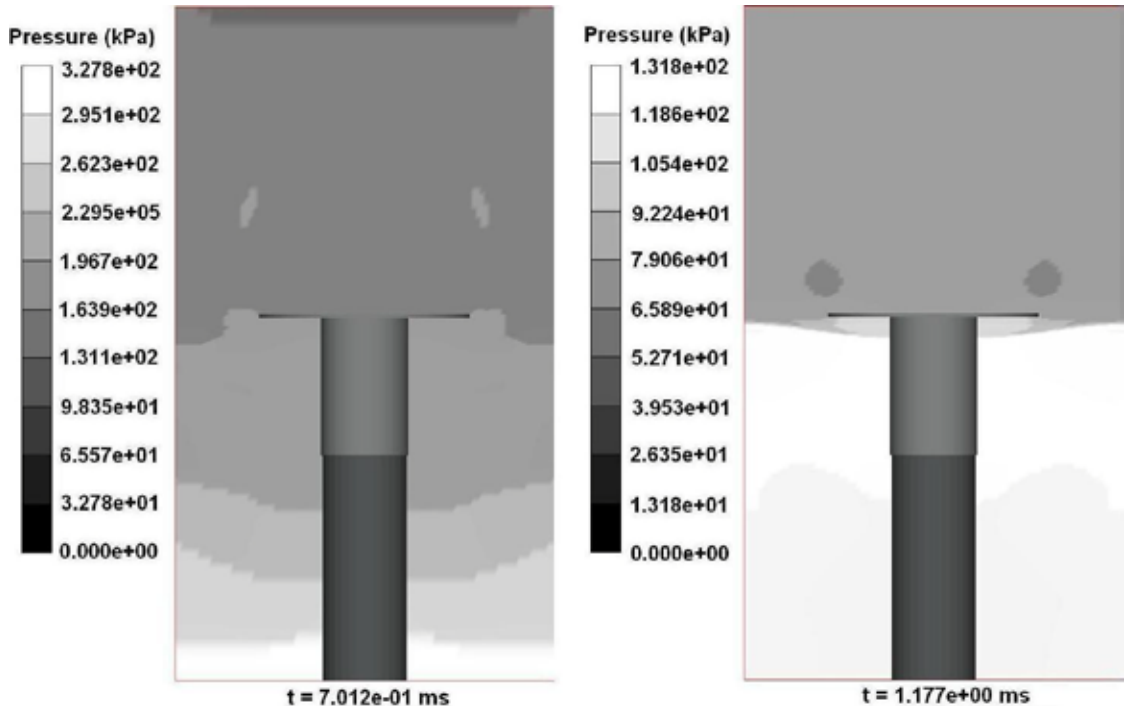

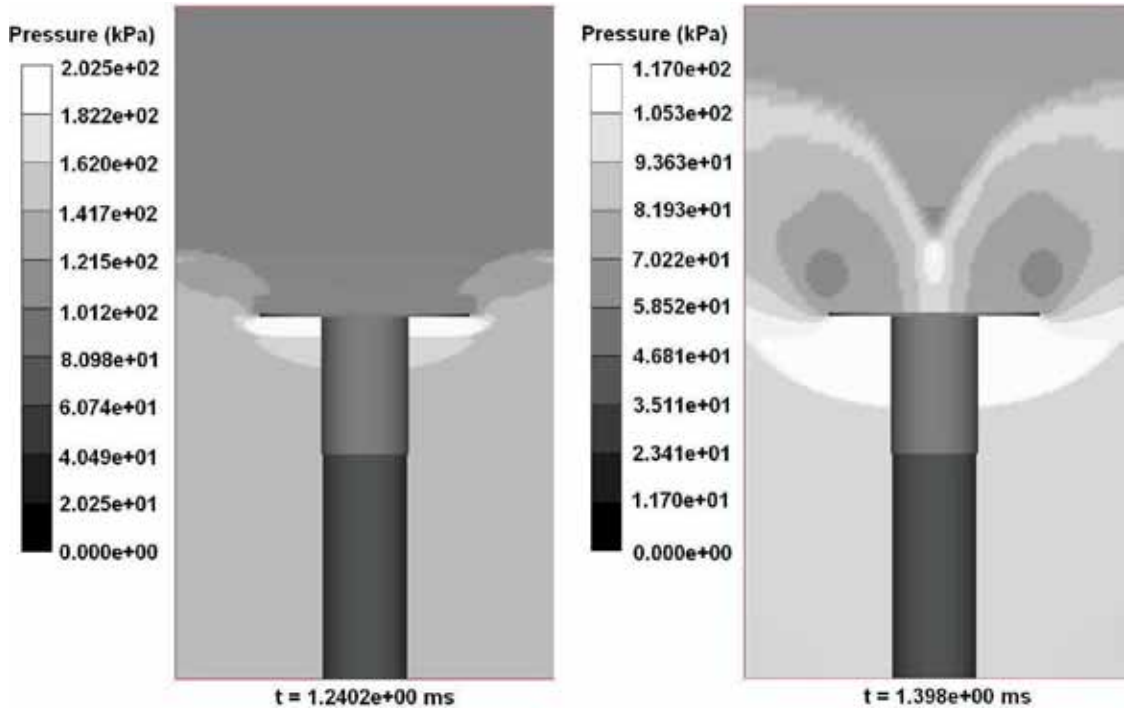

Figure 21: Interaction of the reflected pressure wave with the aluminium skin plate from the ground surface.

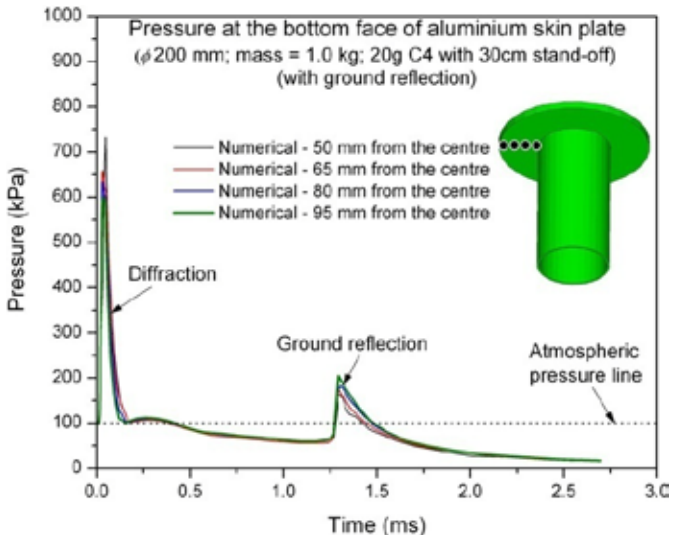

Figure 22: Pressure- time histories at the bottom face of the aluminium skin plate (*f* 200; 1.0kg) with ground reflection.

5.2. Validation of Hydrocodes simulation results

The results from the AUTODYN simulations showed that the total impulse from the diffraction and the ground reflection phenomenon acting at the bottom face of the skin plates was approximately 33% and 30 % of the total reflected impulse for aluminium and sandwich composite skin plates respectively. In order to validate the finding of impulse loss due to diffraction and ground reflection a decoupled analysis was carried out for all cases considering experimentally recorded pressure time histories. Due to the similarity in approach the results of one of the cases (sandwich composite skin plate (*f* 250 mm; 0.36 kg)) are discussed in this section. It was assumed that the proportion of the impulse due to diffraction and ground reflection phenomena (30%) is constant. Figure 23(a) shows one of the experimentally measured reflected pressure - time profile (test 1) on the top face of the

sandwich composite skin plate (f 250 mm; 0.36 kg). The calculated reflected impulse from this curve (area below the reflected pressure time profiles) was 167.7 kPa-ms (0.00823 kN-s). This impulse can be modelled as an equivalent triangular impulse loading which is shown in Figure 23(a) (dashed line). This equivalent triangular impulse load was calculated based on the diffracting (engulfing) load case [18]. The approximate new positive duration for this equivalent triangular impulse load is 0.0663 ms (refer Figure 23(a)). Now, subtracting 30% of the impulse (for diffraction and ground reflection) from the reflected impulse can provide the resultant equivalent triangular impulse (117.4 kPa-ms (0.00576 kN-s)) loading curve; and the corresponding calculated equivalent duration of the resultant triangular impulse load is 0.04645 ms. This resultant load is indicated by the solid line in Figure 23(a). Decoupled numerical analyses have been conducted for these two load cases (dashed line and solid line). The effect of diffraction and ground reflection can be understood from the velocity profile of the sandwich composite skin plate (Figure 23(b)). The velocity profile of the sandwich composite skin plate considering diffraction and ground reflection was close to the experimental data. The corresponding deformation length and its pattern were very close to the experimental data (refer Figure 24(a) and 24(b)). However, the case without considering diffraction and ground reflection showed a higher peak velocity (25.9 m/s) and a lower time (5.32 ms) to reach the zero velocity position (Figure 23(b)). Furthermore, the test specimen crushed completely which is entirely different from the experimental results (refer Figure 24(c)).

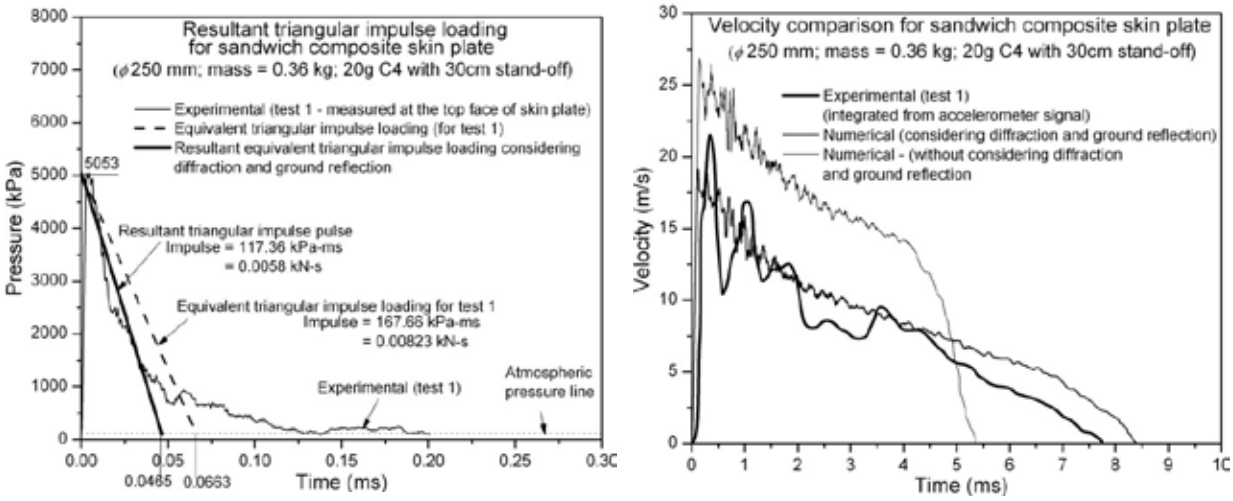

(a) (b)

Figure 23: (a) Simplified equivalent triangular loading. **(b)** Comparison of velocity profiles.

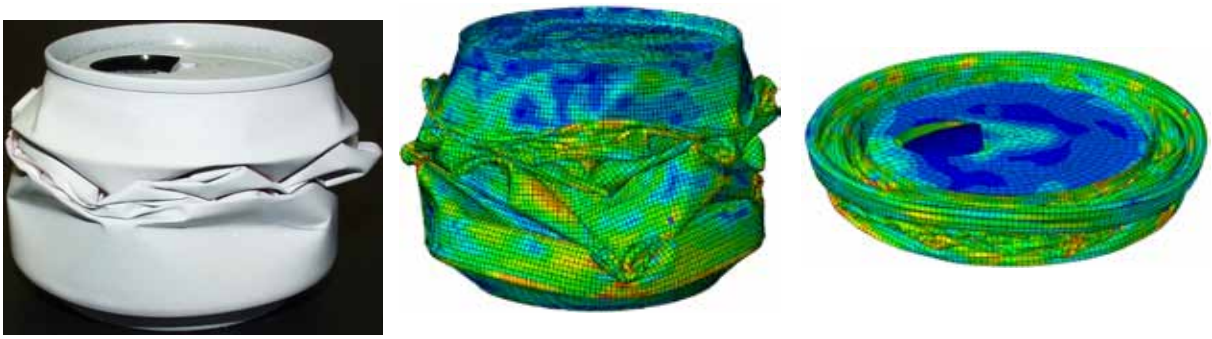

(a) (b) (c)

Figure 24: Deformation patterns of empty recyclable beverage cans with sandwich composite skin plate (f 250 mm; 0.36 kg); **(a)** Experimental **(b)** Numerical (considering diffraction and ground reflection) **(c)** Numerical (without considering diffraction and ground reflection).

The force-deformation curve for the case with diffraction and ground reflection is also shown in Figure 25(a). The peak load from the numerical simulation (3.7 kN) was closer to the experimental data (3.95 kN). Similarly, the calculated total absorbed energy for both cases are comparable (41.96 J and 45.2 J for experimental and numerical respectively). Furthermore, the numerical results of this case showed the conservation of impulse and the energy. Figure 25(b) shows the comparison of the applied equivalent triangular impulse (117.4 kPa-ms (0.0058 kN-s)) and the numerically calculated transferred impulse at the bottom of the beverage can (0.0058 kN-s). The same figure also shows the comparison of energy. It can be noticed that the energy absorbed by the beverage can (45.2 J) was lower than the applied energy to the skin plate by the equivalent triangular impulse load (49.96 J). The difference between these two energy levels was the energy absorbed by the sandwich composite skin plate (by elastic bending of composite skin plates and the compression of polyurethane foam). From the above results it can be concluded that the results yielded by the Autodyn simulations are appropriate.

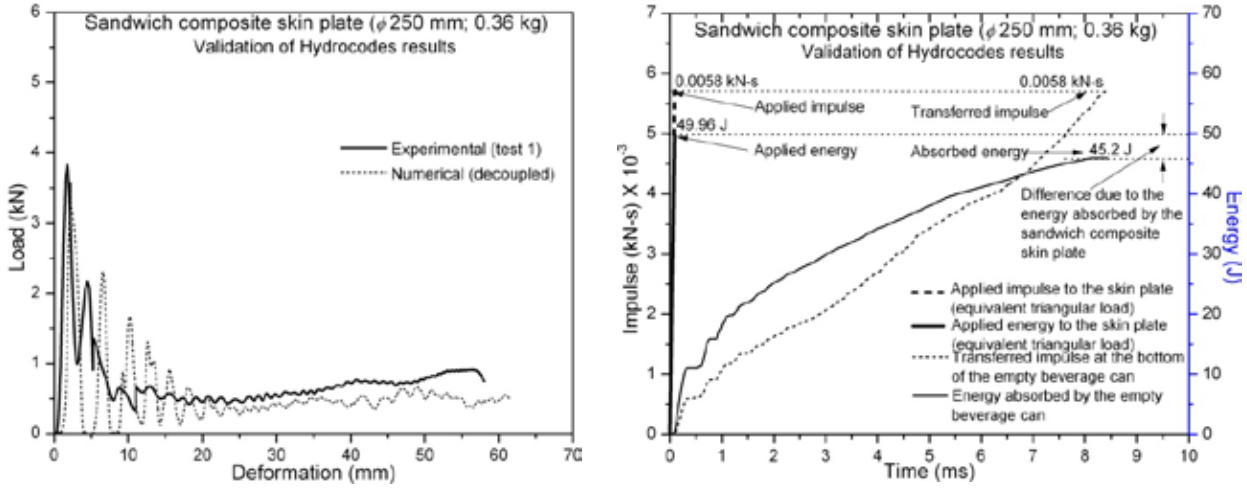

(a) (b)

Figure 25: For sandwich composite skin plate (f 250 mm; 0.36 kg): **(a)** Comparison of force-deformation histories. **(b)** Comparison of impulse and the energy.

6. Conclusions

In this study, the experimental and numerical blast energy absorption characteristics and the corresponding crushing mechanisms of empty recyclable metal beverage cans were investigated. Close-range free-air blast tests have been conducted with 20g of C4 with a stand-off distance of 30 cm. Experiments were carried out with different top skin plates to understand the effect of inertia of the skin plates on the energy absorption of a sacrificial core structure. Furthermore, the effect of the surface area and the nature of the reflected surface on the reflected blast parameters were also evaluated. The experimentally measured blast parameters were compared with predicted values from ConWep. The importance of consideration of the clearing effect of reflected pressure with a finite surface of skin plate was studied. The failure patterns of the empty beverage cans and the corresponding energy absorption levels were studied in detail. From the conducted experiments and numerical simulations the following conclusions can be made:

- The measured values of the peak reflected pressures with aluminium skin plates were lower than the ConWep predicted data. On contrast, the measured peak reflected

pressure values with sandwich composite skin plates were higher than the ConWep values. For both cases the positive duration of the blast event was significantly lower than ConWep predicted data. The difference in the pressure was due to the clearing of the reflected pressure waves associated with the finite surface area of the skin plates. Furthermore, the surface roughness of the reflected surface largely influenced the blast parameters such as peak reflected pressure and positive duration.

- The effect of clearing of the pressure waves has to be considered for the energy absorption evaluation of a sacrificial cladding structure with a finite surface area of the skin plate. Energy absorption prediction with an equivalent triangular impulse load based on empirical relations can over estimate the capacity of the inner core of a sacrificial structure.
- The inertia of the skin plate of a sacrificial cladding structure plays a vital role for the crushing length of the test specimens. A lower mass with adequate bending stiffness of the skin plate would maximize the energy absorption of the inner core structure. The specific energy absorption of an empty beverage can was increased with lower mass of the skin plates.
- The peak crush load of beverage cans with different skin plate mass showed the strain-rate sensitivity. The peak crush load of the beverage cans was approximately three times higher than the quasi-static value. Hence, the effect of increasing strength should be accounted for further investigations.
- The deformation patterns of the empty beverage cans with different skin plate masses were evaluated. Tests with higher inertia and lower surface area of the skin plate showed a plastic local wall buckling along the length of the can. However, tests with lower skin plate masses exhibited uniform formation of lobes around the circumference of the can.
- The 3D computational model showed a clear evidence of clearing of reflected pressure waves with finite surface area of the reflected surface (aluminium and sandwich composite skin plates). The diffracted pressure from the top face quickly passed around the edges and acted on the bottom face of the skin plates. In addition to the diffracted pressure, the incident pressure wave at the boundary of the skin plates also contributed to increase the pressure at the bottom face of the skin plates (engulfing phenomenon). High speed images from the experimental tests also confirmed the same. The magnitude of the diffracted pressure was less than one sixth of the reflected pressure.
- The effect of ground surface reflection on the bottom face of the skin plates was also studied. Approximately 100 kPa (above the atmospheric pressure) was acting on the bottom face of the skin plates due to ground reflection.
- The effective impulse from the diffraction and ground reflection was significant compared to the reflected impulse; an average value of 30% of the reflected impulse acted on the bottom face due to diffraction and ground reflection. The same finding was also validated with a decoupled numerical analysis using experimentally measured pressure time history.

Acknowledgements

The authors gratefully acknowledge the financial support of the “Fund for Scientific Research” – Flanders (F.W.O) (Grant No G.0114.07). The authors appreciate the technical input of Mr. Hicham Echchgadda from M/s Coca cola Ltd, Brussels, Belgium. The authors also wish to thank Luc Van Den Broecke (Ghent University) for his assistance in manufacturing the test set-up.

References

[1] Guruprasad, S. and Mukherjee A., *Layered sacrificial claddings under blast loading Part I -- analytical studies.* International Journal of Impact Engineering, 2000. **24**(9): p. 957-973.

[2] Guruprasad, S. and Mukherjee A., *Layered sacrificial claddings under blast loading Part II -- experimental studies.* International Journal of Impact Engineering, 2000. **24**(9): p. 975-984.

[3] C.Kotzialis, C. D. A. V. K., *Blast behaviour of plates with sacrificial cladding.* 5th GRACM International congress on computational mechanics, 2005.

[4] Hanssen, A. G., Enstock L. and Langseth M., *Close-range blast loading of aluminium foam panels.* International Journal of Impact Engineering, 2002. **27**(6): p. 593-618.

[5] Zou, Z., Tan P. J., Reid S. R., Li S. and Harrigan J. J., *Dynamic crushing of a one-dimensional chain of type II structures.* International Journal of Impact Engineering, 2007. **34**(2): p. 303-328.

[6] Reid, S. R. Y. R. T., *Experimental investigation of inertia effects in one-dimensional metal ring systems subjected to end impact -I. Fixed end systems.* International Journal of Impact Engineering, 1983. **1(1)**: p. 85-106.

[7] R.E.Oshiro, M. A., *Scaling impact structures.* Archive of applied mechanics, 2004. **74**: p. 130-145.

[8] Su, X. Y., Yu T. X. and Reid S. R., *Inertia-sensitive impact energy-absorbing structures part I: Effects of inertia and elasticity.* International Journal of Impact Engineering, 1995. **16**(4): p. 651-672.

[9] Su, X. Y., Yu T. X. and Reid S. R., *Inertia-sensitive impact energy-absorbing structures part II: Effect of strain rate.* International Journal of Impact Engineering, 1995. **16**(4): p. 673-689.

[10] Calladine, C. R. and English R. W., *Strain-rate and inertia effects in the collapse of two types of energy-absorbing structure.* International Journal of Mechanical Sciences, 1984. **26**(11-12): p. 689-701.

[11] Gao, Z. Y., Yu T. X. and Lu G., *A study on type II structures. Part I:: a modified one-dimensional mass-spring model.* International Journal of Impact Engineering, 2005. **31**(7): p. 895-910.

[12] Tam, L. L. and Calladine C. R., *Inertia and strain-rate effects in a simple plate-structure under impact loading.* International Journal of Impact Engineering, 1991. **11**(3): p. 349-377.

[13] Karagiozova, D., Nurick G. N. and Chung Kim Yuen S., *Energy absorption of aluminium alloy circular and square tubes under an axial explosive load.* Thin-Walled Structures, 2005. **43**(6): p. 956-982.

[14] Karagiozova, D. and Alves M., *Transition from progressive buckling to global bending of circular shells under axial impact--Part I: Experimental and numerical observations.* International Journal of Solids and Structures, 2004. **41**(5-6): p. 1565-1580.

[15] Karagiozova, D. and Alves M., *Transition from progressive buckling to global bending of circular shells under axial impact--Part II: Theoretical analysis.* International Journal of Solids and Structures, 2004. **41**(5-6): p. 1581-1604.

[16] Abramowicz, W. and Jones N., *Transition from initial global bending to progressive buckling of tubes loaded statically and dynamically.* International Journal of Impact Engineering, 1997. **19**(5-6): p. 415-437.

[17] P D Smith, J. G. H., *Blast and ballistic loading of structures.* Butterworth-Heinemann Ltd., 1994.

[18] Gilbert F. Kinney, K. J. G., *Explosive shocks in air.* Springer-Verlag, 1985.
[19] S.Palanivelu, W. V. P., J .Degrieck, *Experimental and numerical investigation of axial quasi-static and impact loading of recyclable empty metal beverage cans.* Internal report, Department of Materials Science and Engineering, Ghent University, Belgium, 2008.
[20] Chapman, T. C., Rose T. A. and Smith P. D., *Blast wave simulation using AUTODYN2D: A parametric study.* International Journal of Impact Engineering. **16**(5-6): p. 777-787.
[21] Autodyn, *Theory manual.* M/s Century Dynamics, 2007.
[22] Lesuer, D., *Experimental Investigations of Material Models for Ti-6Al-4V Titanium and 2024-T3 Aluminum.U.S. Department of Transportation.DOT/FAA/AR-00/25,Sept. 2000*
[23] Gordon R.Johnson, W. H. C., *Fracture characteristics of three metals subjected to various strains, strain rates, temperatures and pressures.* Engineering fracture mechanics, 1985. **21**: p. 31-48.
[24] Adelman, S. A. and Doll J. D., *Generalized Langevin equation approach for atom/solid–surface scattering: General formulation for classical scattering off harmonic solids.* Journal of Chemical Physics, 1976. **64**: p. 2375-2388.
[25] Doll, J. D. and Dion D. R., *Generalized Langevin equation approach for atom/solid–surface scattering: Numerical techniques for Gaussian generalized Langevin dynamics.* Journal of Chemical Physics, 1976. **65**(9): p. 3762-3766.
[26] Holmes, N. and Belytschko T., *Post processing of finite element transient response calculations by digital filters.* Computers & Structures, 1976. **6**(3): p. 211-216.
[27] Zekai, C. and Zdenek P. B., *Spurious reflection of elastic waves due to gradually changing finite element size.* International journal of Numerical methods in engineering, 1983. **19**(5): p. 631-646.
[28] Luccioni, B., Ambrosini D. and Danesi R., *Blast load assessment using hydrocodes.* Engineering Structures, 2006. **28**(12): p. 1736-1744.